

A time-dependent description of dissociative excitation of HeH^+

Emelie ERTAN

Department of Chemical Physics
Computational Physics
Master's degree project, 45 HE credits
FK9001
Supervisor: Doc. Åsa LARSON

Stockholm, 2013



Abstract

Acknowledgements

Contents

1	Introduction	2
1.1	Dissociative excitation and related processes	2
1.2	Earlier work on HeH^+	5
2	Theory	8
2.1	The molecular Schrödinger equation and the Born-Oppenheimer approximation	8
2.2	Quantum chemistry and electronic structure calculations	11
2.3	Electron scattering	13
2.4	The adiabatic-nuclei approximation	14
2.5	Complex Kohn variational method	17
2.6	Wave packet methods	21
3	Derivation of cross section	25
3.1	Cross section of photodissociation	25
3.2	Cross section of dissociative excitation	27
3.2.1	Derivation of delta-function approximation	27
3.2.2	Derivation of a time-dependent method	28
4	Computational Details	30
4.1	A note on symmetry	30
4.2	Structure calculations	31
4.3	Electron scattering calculations	31
4.4	Wave packet calculations	32
4.5	Time-independent calculations	32
5	Results	34
5.1	Fixed-nuclei cross section	34
5.2	Effect of resonances	35
5.3	Total cross section of DE obtained using the delta-function approximation	36
5.4	Time-independent cross section using the energy-normalized continuum functions	39
5.5	Time-dependent results	40
5.6	Comparison of time-dependent and time-independent methods	42
6	Discussion	43

7	Concluding Remarks	43
7.1	Further applications of method	43
A	Appendix I	43
A.1	Fourier transformation	43
A.2	The Dirac delta function	44
A.3	The autocorrelation function	45
B	Appendix II - Convergence testing of the wave packet model	47
C	Appendix III - Conventions and notations	51

1 Introduction

This work describes a time-dependent theoretical study of *dissociative excitation* (DE) of the molecular HeH^+ ion. Using wave packet analysis, a numerical model for calculating the cross section of the DE process will be developed. The theoretical background for this project will include molecular physics such as electron scattering and dissociation dynamics as well as numerical methods, computational physics and data processing techniques. This means that we have to be able to change quickly from theoretical physics to a computational viewpoint and both parts must be given equal attention. This paper will therefore, in addition to the theoretical part, include detailed descriptions of the computational methods that are used.

In this section the DE process as well as other related electron scattering processes will be presented. Results of earlier studies of DE of HeH^+ , both theoretical and experimental, will also be discussed and these will serve as a background for this work.

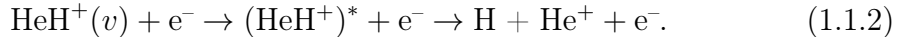
1.1 Dissociative excitation and related processes

Dissociative excitation is the process wherein a molecular ion is promoted to an electronically excited state by collision with an electron. If the excited state has a repulsive potential it dissociates immediately to fragments where one is neutral and the other ionic. The general formulation of the DE process for a diatomic molecular ion is given as follows,



Dissociative excitation is generally studied using beam methods and the most common target is the hydrogen molecular ions [1]. While other related electron scattering processes have been relatively well studied, DE has not received equal attention.

In this work the DE process is studied theoretically for the HeH^+ system. The ground state of HeH^+ is the $X^1\Sigma^+$ state with an equilibrium distance of about $1.45 a_0$, and it dissociates to $\text{He} + \text{H}^+$. In order for dissociation into other atomic fragments to occur, the system must be promoted into an electronically excited state. Here, the following direct DE process of HeH^+ is studied:



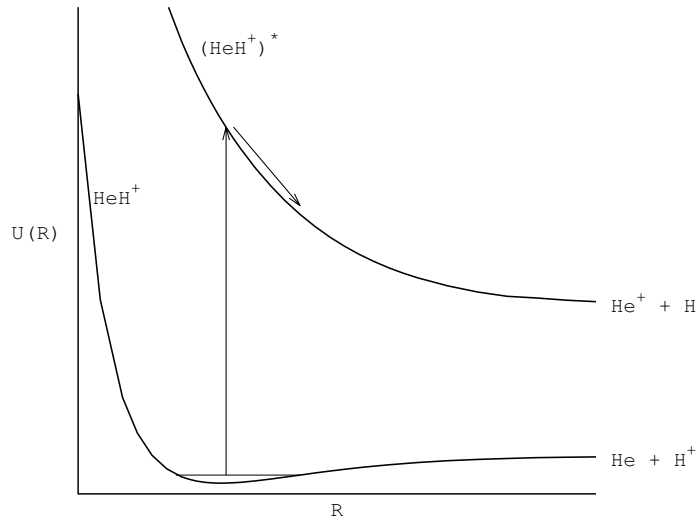


Figure 1: Schematic diagram of the dissociative excitation process in the case of the HeH^+ . The system is excited by inelastic electron scattering from the ground state to an excited state $(\text{HeH}^+)^*$ from where the system dissociates to $\text{He}^+ + \text{H}$.

The direct DE process for HeH^+ is displayed schematically in Fig. 1.

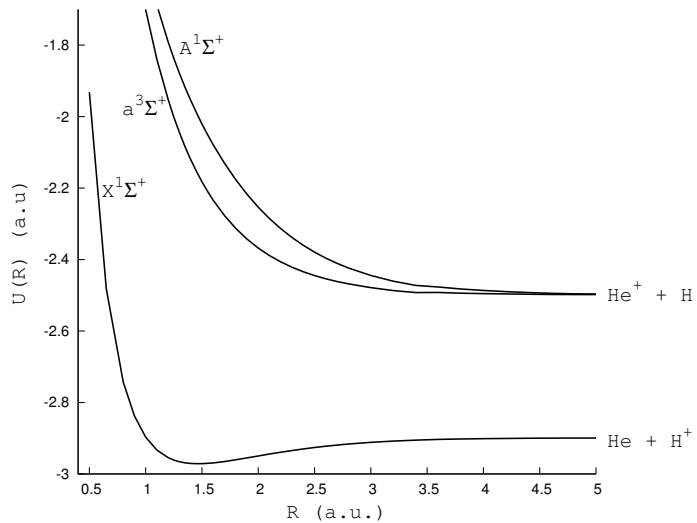


Figure 2: The potential energy curves of the ground state ($X^1\Sigma^+$), the first excited state ($a^3\Sigma^+$) and the second excited state ($A^1\Sigma^+$) of HeH^+ . Both excited states dissociate to $\text{He}^+ + \text{H}$, while the ground state dissociates to $\text{He} + \text{H}^+$.

The first excited state of HeH^+ is the $a^3\Sigma^+$ state, which is repulsive and dissociates into $\text{H} + \text{He}^+$. The second excited state is the $A^1\Sigma^+$ state, which is

also a repulsive state dissociating into the same limit. The potential energy curves of the ground state and the two first excited states are displayed in Fig. 2.

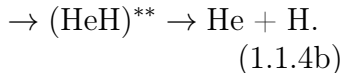
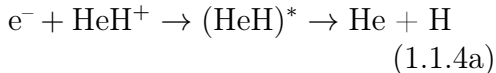
Dissociative excitation of HeH^+ has previously been studied experimentally [3, 4] as well as theoretically [2] and the results form the background for this work. More details on the earlier work will be given in the following section. A property of interest is the absolute cross section of the reaction. By both experiment and theory it has been shown that the cross section of DE of HeH^+ is very small compared to that of *Dissociative recombination* (1.1.4) at low energy [2, 3, 4].

Experimental studies have revealed the existence of an alternate DE pathway, called *Resonant dissociative excitation* [4]. This process has also been studied theoretically [5]. This reaction is expressed as follows for HeH^+



In this process the electron is captured into a Rydberg state to an excited ionic core, forming a doubly excited neutral state, which in turn autoionizes back into the ground electronic state of HeH^+ . If it is autoionizing to a nuclear continuum level, it will have enough energy to dissociate. It should be noted that this reaction has a threshold of about 10 eV, while the direct process has a threshold above 16 eV [4].

Another dissociation process is *Dissociative recombination* (DR), which for HeH^+ is given by



In (1.1.4) the collision with the electron occurs at a low energy compared to the DE in (1.1.2). Below 10 eV, the DR reaction of HeH^+ is driven by capture into Rydberg states with potential energy curves situated below the ground ionic state [Eq. (1.1.4a)].

When an electron is excited to a molecular orbital far away from the nuclei, the electron experiences almost a spherical potential and the potential energy curve can be approximated using the energy levels of the hydrogen atom, *i.e.*,

$$V_n(R) \sim V_{\text{ion}}(R) - \frac{1}{2n^2},$$

where the principal quantum number $n = 2, 3, 4, \dots$

However, the potential that the nuclei experiences is not completely spherical and the deviation causes a quantum defect, $\mu_\ell(R)$, such that an effective principal quantum number is obtained,

$$n_\ell^{\text{eff}} = n - \mu_\ell(R).$$

Here, ℓ is the electronic angular quantum number. An infinite series of states, called **Rydberg states**, exist where the potential of the individual states is given by

$$V_{\text{nc}}(R) = V_{\text{ion}}(R) - \frac{1}{2(n - \mu_\ell(R))^2}.$$

Above 10 eV, the energy is high enough for capture into the doubly excited state of HeH [Eq. (1.1.4b)] and the DR and the resonant DE are competing processes [4].

1.2 Earlier work on HeH⁺

As it was mentioned in subsection 1.1 there has not been as much work done on DE as on other related processes, such as dissociative recombination. The most common systems studied for DE is the hydrogen molecular ion. However, since HeH⁺ is a quite small system, it has also gained some previous attention. In the scope of this project both earlier experimental and theoretical works have been studied in order to gain insight in the DE process of HeH⁺ and have been used as comparison for the result obtained using our method. Some of these studies have already been referred to in subsection 1.1.

One of the earliest published experimental studies on DE of HeH⁺ is the work of F. B. Yousif and J. B. A. Mitchell from 1989 [3]. In this work the DR and DE processes of HeH⁺ were studied using a merged beam method. Yousif and Mitchell reported the cross sections for DE in the 0 – 40 eV energy range. The results showed an excitation energy threshold at about 20 eV for the low extraction conditions, where the ions are believed to be mainly in the ground electronic state. Series of sharp and very narrow peaks in the cross section were detected in the 20 – 26 eV energy region. The narrowness of the peaks was suggested to originate from a process where the electron is trapped instantaneously into doubly excited neutral resonant states.

The findings of Yousif and Mitchell prompted the theoretical study by A. E. Orel, T. N. Rescigno and B. H. Lengsfeld III [2]. In this work the DE of HeH⁺ was studied in the 20 – 26 eV energy region using the *complex Kohn variational method* [10, 14]. Excitation cross sections for the $X^1\Sigma^+ \rightarrow a^3\Sigma^+$ transition were computed in overall $^2\Sigma^+$ and $^2\Pi$ symmetries as well as the total cross section at the equilibrium separation ($R_0 = 0.77 \text{ \AA}$). The calculation of the fixed-nuclei cross section resulted in a series of sharp peaks on a quite flat background. Closer inspection showed that most of the peaks were Feshbach resonances associated with energetically closed Rydberg states in this energy region. One of the peaks, situated at 24 eV, did not belong to the above mentioned category but proved to be a core-excited shape resonance. Further, in the work of A. E. Orel, T. N. Rescigno and B. H. Lengsfeld III [2], it was shown that an auto-ionization process from an doubly excited state, as suggested by Yousif and Mitchell, was not a viable explanation of the narrowness of the peaks observed in the experiment.

The computations in $^2\Sigma^+$ symmetry were also preformed at $R = R_0 \pm 0.05 \text{ \AA}$ in order to investigate how the cross section responds to changes in the internuclear distance. The results from these calculations showed that the widths of the resonance peaks and the value of the background cross section remained almost

unchanged. The positions of the peaks were shifted with the excitation energy of the $X^1\Sigma^+ - A^1\Sigma^+$ transition.

In this work a formula for calculating the averaged fixed-nuclei cross section was also derived as follows

$$\sigma(E_0) = \int \sigma(E_0, R) [\chi_{\nu_0}(R)]^2 dR. \quad (1.2.1)$$

Here χ_{ν_0} is the initial target vibrational wave function and $\sigma(E_0, R)$ is the "fixed-nuclei cross section". This formula, which will be presented and explained in more detail in the Theory subsection 3.2, will be implemented in the scope of the present work.

When an averaged total excitation cross section was calculated, the R -dependence of the excitation thresholds could therefore be included as a shift with respect to R_0 and the sharp peaks observed in the fixed-nuclei cross section were smoothed out.

A second experimental study of the DE of HeH^+ was performed by C. Strömholm *et al.* [4]. In this work the DR and DE processes for HeH^+ were studied and the absolute cross sections were determined for energies below 40 eV. The experiments were performed using CRYRING at the Manne Siegbahn Laboratory at Stockholm University. Contrary to the results of the cross section obtained by Yousif and Mitchell, it was found here that the absolute cross section for the direct DE process was basically constant in the 21–37 eV energy region. Furthermore, it was found that there was an alternate DE pathway with an energy threshold already at 10 eV. In the reaction the electron gets caught up in a neutral doubly excited state which auto-ionizes into $\text{He} + \text{H}^+$. This reaction is the *resonant dissociative excitation* presented in subsection 1.1 and, as described above, it competes with the DR process.

The results of the direct DE cross section for the HeH^+ of the above mentioned studies are displayed in Fig. 3.

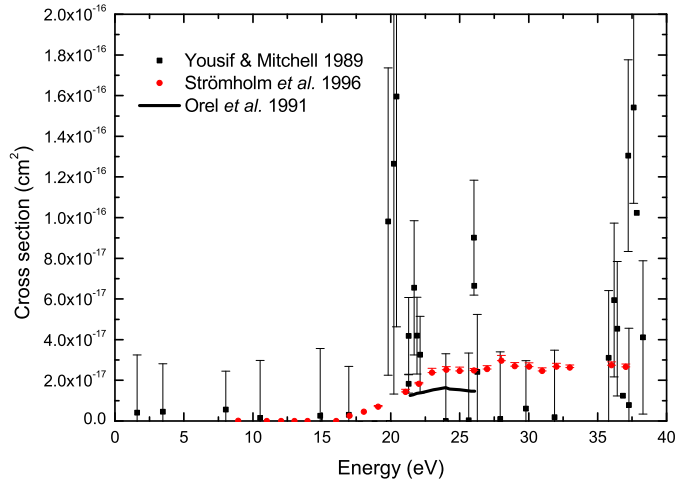


Figure 3: Previous results for the cross section of the direct DE of HeH^+ obtained from the experimental works of Yousif and Michell [3], Strömholm *et al.* [4] and a theoretical study of Orel *et al.* [2].

The results of Strömholm *et al.* were soon discussed in a theoretical study by A. E. Orel and K. C. Kulander [5]. Here the resonant DE mechanism was investigated using the complex Kohn variational method and wave packet calculations. The theoretical results showed good agreement with the experimental results for the dissociation threshold, however, the calculated cross sections exhibited a magnitude nearly twice as large as that of the experimental data. It was discussed that this discrepancy may have been caused by non-adiabatic coupling of the resonant states to excited ion states¹.

¹In later work [6], the cross section was formulated without a factor 2, suggesting that the original expression may have been incorrect.

2 Theory

In this section the theoretical background relevant for this work will be related. The aim of this project is to develop a model using wave packets to describe the direct dissociative excitation process of HeH^+ . Therefore the main focus of this section will be to present the background of wave packet dynamics and the theory necessary to understand the derivation of the cross section in section 3.

Even though it is far too complex to be related in full in the scope of this work some basic theory of electron scattering as well as a short introduction to the *complex Kohn variational method* (CKVM) [10] is included in this section. Neither of these topics are comprised in the head part of this project, nevertheless, I feel that a basic understanding is necessary to fully grasp the theoretical background of this work.

This section starts with a brief introduction of the *Born-Oppenheimer* (BO) *approximation* [11] followed by a short presentation of *quantum chemistry*, where specifically the *Multi-Reference Configuration Interaction* (MRCI) method is discussed. Note that atomic units ($\hbar = e = m_e = a_0 = 1$) are used throughout. For more details, conversion factors *etc.* see Appendix III - Conventions and notations.

2.1 The molecular Schrödinger equation and the Born-Oppenheimer approximation

If the spin-orbit and relativistic interactions of the nuclei and electrons is neglected, the molecule can be described by means of the time-*independent* Schrödinger equation:

$$H\psi(\mathbf{R}, \mathbf{r}) = E_{\text{tot}}\psi(\mathbf{R}, \mathbf{r}). \quad (2.1.1)$$

For this molecular system the Hamiltonian can be partitioned in the following manner

$$H = T_{\text{N}} + H_{\text{e}} + V_{\text{NN}}, \quad (2.1.2)$$

where T_{N} is the kinetic energy operator of the nuclei and V_{NN} is the nuclear repulsion term. H_{e} , called the *electronic Hamiltonian*, consists of the kinetic energy operator of the electrons as well as the electron-electron and electron-nuclei interactions. These terms can be expressed as follows.

$$\begin{aligned} T_{\text{N}} &= -\frac{1}{2\mu} \nabla_{\text{R}}^2 \equiv T_{\text{vib}} + T_{\text{rot}} \\ H_{\text{e}} &= -\frac{1}{2} \sum_i^N \nabla_i^2 - \sum_{\alpha}^2 \sum_i^N \frac{Z_{\alpha}}{r_{\alpha i}} + \sum_i^N \sum_{j>i}^N \frac{1}{r_{ij}} \\ V_{\text{NN}} &= \frac{Z_{\alpha} Z_{\beta}}{R}. \end{aligned} \quad (2.1.3)$$

Here the vibrational part of the nuclear kinetic energy operator is given by

$$T_{\text{vib}} = -\frac{1}{2\mu R^2} \frac{\partial}{\partial R} \left(R^2 \frac{\partial}{\partial R} \right) \quad (2.1.4)$$

and the rotational part by

$$T_{\text{rot}} = -\frac{1}{2\mu R^2} \left[\frac{1}{\sin \theta} \frac{\partial}{\partial \theta} \left(\sin \theta \frac{\partial}{\partial \theta} \right) + \frac{1}{\sin^2 \theta} \frac{\partial}{\partial \varphi^2} \right]. \quad (2.1.5)$$

The reduced mass for nuclei α and β is defined as $\mu = m_\alpha m_\beta / (m_\alpha + m_\beta)$. Indices i and j refer to the electrons and Z_α is the atomic number of nuclei α . It is common to introduce a center of mass coordinate system. For a diatomic molecule with the center of mass will be situated in between the two nuclei, coinciding with the origin and the motion of N electrons is given by $\mathbf{r} = \{\mathbf{r}_1, \mathbf{r}_2, \dots, \mathbf{r}_N\}$ and the internuclear distance is defined by $R = |\mathbf{R}_\alpha - \mathbf{R}_\beta|$. Here \mathbf{R}_α and \mathbf{R}_β are the positions of atoms α and β . $r_{\alpha i}$ represents the distance between nuclei α and electron i and r_{ij} is the distance between electrons i and j . $r_{\alpha i}$, r_{ij} and R are illustrated in Fig. 4 for a diatomic molecule with 2 electrons.

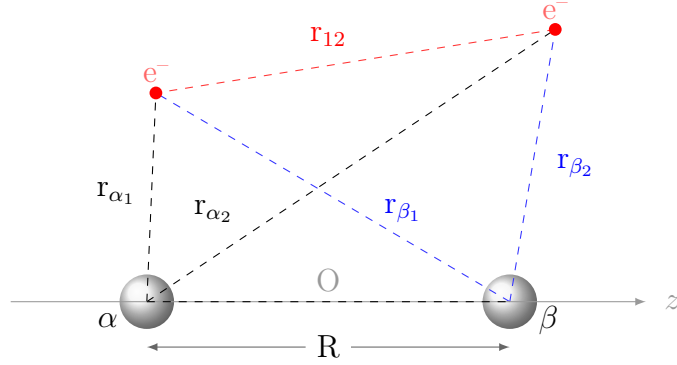


Figure 4: Schematic figure of a diatomic system with two electrons.

The eigenvalues to Eq. (2.1.1) can be obtained by the following expansion

$$\psi(\mathbf{R}, \mathbf{r}) = \sum_i \psi_{ni}(\mathbf{R}) \psi_{ei}(\mathbf{R}, \mathbf{r}), \quad (2.1.6)$$

where ψ_{ni} only depends on R . Here ψ_{ei} are the solutions to the *electronic Schrödinger equation* at fixed internuclear distances,

$$H_e \psi_{ei}(\mathbf{R}, \mathbf{r}) = U_i(R) \psi_{ei}(\mathbf{R}, \mathbf{r}). \quad (2.1.7)$$

The nuclear repulsion term V_{NN} is usually included in H_e and the electronic Hamiltonian depends parametrically on the internuclear distance, R . The eigenvalues

to the electronic Schrödinger equation for the diatomic molecule form a *potential energy curve* $U_i(R)$ of state i .

If Eqs. (2.1.2) and (2.1.6) are substituted into Eq. (2.1.1), the following expression is obtained

$$[T_N(\mathbf{R}) + H_e(\mathbf{R}, \mathbf{r})] \sum_i \psi_{ni}(\mathbf{R}) \psi_{ei}(\mathbf{R}, \mathbf{r}) = E \sum_i \psi_{ni}(\mathbf{R}) \psi_{ei}(\mathbf{R}, \mathbf{r}). \quad (2.1.8)$$

Multiplying Eq. (2.1.8) with the electronic wave function ψ_{ej}^* and integrating over electronic coordinates yields the following expression

$$\sum_i \langle \psi_{ej} | T_N + H_e | \psi_{ni} \psi_{ei} \rangle = \sum_i \langle \psi_{ej} | E | \psi_{ni} \psi_{ei} \rangle. \quad (2.1.9)$$

Further, using the orthonormality, $\langle \psi_{ei} | \psi_{ej} \rangle = \delta_{ij}$, and Eq. (2.1.7) we get

$$\sum_i \langle \psi_{ej} | T_N | \psi_{ni} \psi_{ei} \rangle + U_j \psi_{nj} = E \psi_{nj}, \quad (2.1.10)$$

where $j = 1, 2, 3, \dots$. Eq. (2.1.10) is referred to as the nuclear Schrödinger equation in the adiabatic representation. Evaluation of the first term of Eq. (2.1.10) will give rise to an infinite number of coupled differential equations for ψ_{ni} . These equations cannot generally be solved analytically and approximations of the system must be made.

The Laplace operator of T_N will affect both ψ_{ni} and ψ_{ei} as they both are \mathbf{R} dependent. Because of this the chain rule have to be applied on $\psi_{ni} \psi_{ei}$ and we get derivatives of both the nuclear and the electronic wave functions,

$$\begin{aligned} \langle \psi_{ej} | T_N | \psi_{ni} \psi_{ei} \rangle &= -\frac{1}{2\mu} \langle \psi_{ej} | \nabla_{\mathbf{R}}^2 | \psi_{ni} \psi_{ei} \rangle = -\frac{1}{2\mu} \langle \psi_{ej} | \nabla_{\mathbf{R}} \cdot (\nabla_{\mathbf{R}} \psi_{ni} \psi_{ei} + \psi_{ni} \nabla_{\mathbf{R}} \psi_{ei}) \rangle \\ &= -\frac{1}{2\mu} [\langle \psi_{ej} | \psi_{ei} \rangle \nabla_{\mathbf{R}}^2 \psi_{ni} + 2 \langle \psi_{ej} | \nabla_{\mathbf{R}} \psi_{ei} \rangle \cdot \nabla_{\mathbf{R}} \psi_{ni} + \langle \psi_{ej} | \nabla_{\mathbf{R}}^2 \psi_{ei} \rangle \psi_{ni}]. \end{aligned} \quad (2.1.11)$$

Within the BO approximation we assume that T_N operator has no effect on the electronic wave function, meaning that non-adiabatic coupling elements $\langle \psi_{ej} | \nabla_{\mathbf{R}} \psi_{ei} \rangle$ and $\langle \psi_{ej} | \nabla_{\mathbf{R}}^2 \psi_{ei} \rangle$ can be neglected. This is a feasible assumption as the large difference in particle weight makes the nuclei practically stationary compared to the electrons. Using the BO approximation and the orthonormality of the electronic states, Eq. (2.1.10) is simplified to

$$(T_N + U_j(R)) \psi_{nj}(\mathbf{R}) = E \psi_{nj}(\mathbf{R}). \quad (2.1.12)$$

Thus, Eq. (2.1.12) provides a set of uncoupled equations for ψ_{ni} , which is the nuclear wave function for the state i . The total wave function can now be obtained according to Eq. (2.1.6)

$$\psi(\mathbf{R}, \mathbf{r}) = \psi_n(\mathbf{R}) \psi_e(\mathbf{r}, \mathbf{r}). \quad (2.1.13)$$

The Born-Oppenheimer approximation is usually valid for electronic ground states that are well separated in energy from excited states. But for certain systems the BO approximation is not always applicable. A system engaged with an ionic bond will experience problems; at equilibrium distance the bond is essentially ionic A^+B^- , however, at large separation the bond will instead be of covalent type. At a certain internuclear distance the potential energy curve of the covalent state becomes very close to the energy of the ionic state. For a diatomic molecule the potential energy curves of the same electronic symmetry are not allowed to cross [12], instead an avoided crossing is formed where the electronic wave function change character going from one side of the avoided crossing to the other. Close to the avoided crossing the non-adiabatic couplings are large and the BO approximation breaks down.

2.2 Quantum chemistry and electronic structure calculations

The electronic Schrödinger equation can only be solved analytically for one-electron systems, such as the H_2^+ . For larger systems we have to rely on approximate methods. These methods use the variational principle to find approximate solutions to the electronic Schrödinger equation, so called trial wave functions, Φ_T , that are energy minimized with respect to some parameters in the trial wave function. The energy for normalized wave functions are given as

$$E_e = \langle \Phi_T | H_e | \Phi_T \rangle, \quad (2.2.1)$$

We assume that the wave function, Φ_0 gives the lowest energy E_0 and we want to determine the parameters of this wave function. A solution to the electronic Schrödinger equation has to obey the Pauli principle, i.e. the total wave function must change sign under permutation of electrons. To construct wave function that behaves in this manner a Slater determinant is set up,

$$\Phi(1, 2, \dots, N) = \frac{1}{\sqrt{N!}} \begin{vmatrix} \phi_1(1) & \phi_2(1) & \dots & \phi_N(1) \\ \phi_1(2) & \phi_2(2) & \dots & \phi_N(2) \\ \vdots & \vdots & \ddots & \vdots \\ \phi_1(N) & \phi_2(N) & \dots & \phi_N(N) \end{vmatrix}. \quad (2.2.2)$$

The elements in the Slater determinant are one-particle molecular orbitals (MO's) made up of a spin part and a spatial part, so called spin orbitals,

$$\phi(i) = \psi(r_i) |s\rangle. \quad (2.2.3)$$

The spin function, has two possible alignments, α and β .

There are many approaches to derive a trial wave function where the main difference is how the electron correlation is included.

One method is the *Configuration Interaction* (CI) method. In standard CI the wave function is made up a linear combination of Slater determinants, also called *Configurational State Functions* (CSF's), corresponding to different configurations where electrons have been excited, a so called configurational expansion.

$$\Psi_{\text{CI}} = \sum_i c_i \Phi_i \quad (2.2.4)$$

The first term in the expansion corresponds to a Slater determinant where all electrons are in their ground state configuration. The Slater determinants in the following terms correspond to different configurations where electrons are excited from the ground state, *see* Fig. 5. In full CI all possible configurations are included and therefore, if a complete basis set is used, $\Psi_{\text{CI}} = \Psi_{\text{exact}}$. The coefficients c_i are determined independently using variational methods, but the determinants are held constant. The coefficients give the weight of the determinants, *i.e.* the configurations.

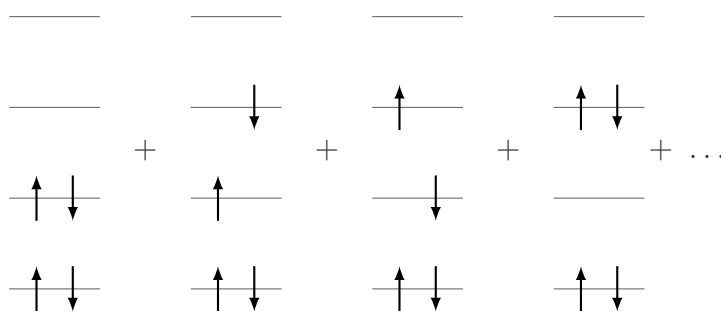


Figure 5: CSF from linear combination of Slater determinants.

In *Multi-Configurational Self-Consistent Field* (MCSCF) not only the expansion coefficients but also the molecular orbitals used to construct the Slater determinants are optimized. This way the most important configurations can be included in the wave function. As implied by the name the MCSCF optimization is an SCF procedure². MCSCF methods have problems with slow convergence and the difficulty to recover correlation energy. One option to remedy some of the electron correlation problem is to allow for configurations where there are some orbitals that are singly occupied, *i.e.* excitation of electrons in the active space (*see*

²The orbital equations are solved in an iterative manner for an initial guess and after each iteration a new solution can be formed. When the convergence criteria (self-consistency) is reached, the procedure will terminate.

Fig. 6). This is called a near-degeneracy effect, meaning that there are configurations with approximately the same energy. This process will recover some of the correlation energy and with appropriate choice of configurations, one can manage to include correlation that is of importance to different properties. The remaining part of the electron correlation cannot be obtained using MCSCF methods. MCSCF is thus a method highly reliant on the appropriate choice of configurations and orbitals used. Another important factor in MCSCF is the definition of the size of the active space; depends on the system at hand. The orbitals for *Multi Reference Configuration Interaction* (MRCI) are usually obtained from MCSCF calculations. Multi-reference refers to the CSF's in the method being generated with several determinants. In MRCI electrons are excited into virtual orbitals and by combining MRCI with MCSCF, correlation lacking from the MCSCF methods can be recovered.

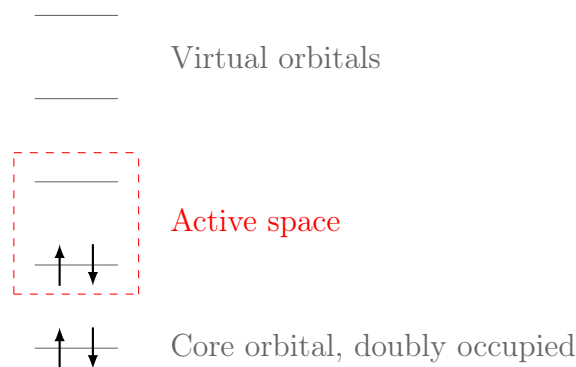


Figure 6: The active space is defined differently depending on the method. Sometimes all occupied orbitals, as well as some of the lower unoccupied orbitals are included (CASSCF). The active space can also be divided, where each part includes a restricted number of orbitals (RASSCF).

2.3 Electron scattering

The dissociative excitation process is essentially an *inelastic* electron scattering process where, if scattering energy is sufficient, the system is promoted into an excited electronic state. This means that the momentum of the incoming electrons, k_n , is not equal to that of the scattered electrons, $k_{n'}$, as opposed to an *elastic* scattering process where $k_n = k_{n'}$. The final state of the system is dependent of the amount of scattering energy that is supplied; if it is small the system might only reach the first excited state or the scattering process becomes elastic, if it is great the system can reach higher excited states.

A scattering process where excitation is possible is said to be *multi-channel* and the different final states are called *channels*. A channel is called open if the supplied scattering energy is sufficient to bring the system into the state. In this work we only consider the first and second excited electronic states of HeH⁺ (see Fig. 2), in other words $n' = 1, 2$ and we study the inelastic scattering $0 \rightarrow 1$ and $0 \rightarrow 2$.

It is common to study the electron scattering process through means of the *differential cross section* and for the transition $n \rightarrow n'$ it is given by

$$\left(\frac{d\sigma}{d\Omega}\right)_{n \rightarrow n'} = \frac{k_{n'}}{k_n} |f_{n'n}(\mathbf{k}', \mathbf{k})|^2. \quad (2.3.1)$$

For the simplest case, elastic scattering, the differential cross section is simply given as the ratio of the scattered particles into the solid angle, $d\Omega$, and the total number of incoming electrons per unit area. This ratio can be given by the square of the *scattering amplitude*, $f_{n'n}(\mathbf{k}', \mathbf{k})$. Another observable related to the differential cross section is the *total cross section*, which is obtained by integrating the differential cross section over all solid angles,

$$\sigma_{n \rightarrow n'} = \int \left(\frac{d\sigma}{d\Omega}\right)_{n \rightarrow n'} d\Omega = \int \frac{k_{n'}}{k_n} |f_{n'n}(\mathbf{k}', \mathbf{k})|^2 d\Omega. \quad (2.3.2)$$

In this work the total inelastic scattering cross section will be calculated.

2.4 The adiabatic-nuclei approximation

In calculation of elastic electron scattering it is commonly assumed that the nuclei can be held fixed in space throughout the complete scattering process. This is a feasible approximation, as the velocity of the incoming electron is considerably faster than the rotational and vibrational motions of the nuclei [8]. It cannot be freely assumed that the fixed-nuclei approximation is applicable for all scattering processes. However, electron scattering with a sufficiently high impact energy will make the motions of the nuclei seem slow compared to the incident electron and the nuclei position can be assumed fixed during the process. This theory is known as the *adiabatic-nuclei approximation* and it was first derived by Chase 1956 [7] in the field of nuclear physics. The model of Chase has proven to be successfully applicable also to electron-molecule scattering processes [8].

The original adiabatic-nuclei approximation is derived not only for fixed nuclei but also for fixed target electrons. However, in electron-molecule scattering, these electrons must be allowed to move if we want to describe electronic excitation of the target. Based on the existing adiabatic-nuclei approximation, Shugard and

Hazi [9] developed in the 1970s a more general theory for the non-resonant scattering process of an electron and a neutral molecule where target excitation was included. The studied inelastic scattering processes, such as

$$AB(n_i, v_i, J_i) + e^- \rightarrow AB(n_f, v_f, J_f) + e^-. \quad (2.4.1)$$

Here, (n_j, v_j, J_j) refer to the quantum numbers of the electronic, vibrational and rotational levels of the system.

The outlines of this theory, that are also applicable to electron-molecular ion scattering processes, will now be presented.

The adiabatic-nuclei approximation is applicable in scattering processes where the incoming electron has a high energy [9]. When the nuclei are fixed the total Hamiltonian will reduce to the electronic Hamiltonian,

$$H_{\text{el}}^{(N+1)}\psi(\mathbf{r}, \mathbf{r}', \mathbf{R}) = \varepsilon(R)\psi(\mathbf{r}, \mathbf{r}', \mathbf{R}). \quad (2.4.2)$$

Here, \mathbf{r} and \mathbf{r}' refer to the coordinates of scattered and the target electrons, respectively. The discrete solutions to Eq. (2.4.2) correspond to bound electronic states of the neutral molecular system. A set of continuum solutions are also obtained, describing the scattering in the fixed-nuclei framework. The solutions to target's bound states are given by electronic Schrödinger equation,

$$H_{\text{el}}^{(N)}\phi_n(\mathbf{r}', \mathbf{R}) = \epsilon_n(R)\phi_n(\mathbf{r}', \mathbf{R}). \quad (2.4.3)$$

The scattering solutions $\psi_{\varepsilon\Omega n_i}^+$ of Eq. (2.4.2) can be formulated asymptotically in the following manner

$$\psi_{\varepsilon\omega n_i}^+ \underset{r \rightarrow \infty}{\sim} k_n^{1/2} (2\pi)^{-3/2} \sum_{n'} \left[\delta_{nn'} e^{i\mathbf{k}_n \cdot \mathbf{r}} - (2\pi)^2 (k_n k_{n'})^{-1/2} t_{n'n}(\omega', \omega; \mathbf{R}) \frac{e^{ik_{n'} r}}{r} \right] \phi_{n'}(\mathbf{r}', \mathbf{R}), \quad (2.4.4)$$

where the incident and final momentum vectors, \mathbf{k}_n and $\mathbf{k}_{n'}$ of the scattering electron have their orientations specified by ω and ω' , respectively. The initial and final electronic states are labeled by n and n' and $t_{n'n}(\omega', \omega; \mathbf{R})$ is the fixed-nuclei scattering amplitude, as defined by Shurgard and Hazi. The total electronic energy, ε , is determined by

$$\varepsilon = \epsilon_n(R) + \frac{1}{2}k_n^2 \quad (2.4.5)$$

and energy conservation gives

$$\frac{1}{2}k_{n'}^2 = \frac{1}{2}k_n^2 + \epsilon_n(R) - \epsilon_{n'}(R). \quad (2.4.6)$$

For a system such as this, the total scattering wave function can be obtained as follows [9]

$$\Psi_{En_i\nu_i J_i}^+(\mathbf{r}, \mathbf{r}', \mathbf{R}) = \psi_{\varepsilon\Omega n_i}^+(\mathbf{r}, \mathbf{r}', \mathbf{R}) F_{n_i\nu_i J_i}(\mathbf{R}). \quad (2.4.7)$$

Here $F_{n\nu J}$ are the nuclear functions of the Born-Oppenheimer product, defined as $\phi_n(\mathbf{r}', \mathbf{R})F_{n\nu J}(\mathbf{R})$, and satisfy

$$\left[-\frac{1}{2\mu} \nabla_{\mathbf{R}}^2 + \epsilon_n(R) - \bar{w}_{n\nu J} \right] F_{n\nu J}(R) = 0, \quad (2.4.8)$$

where $\bar{w}_{n\nu J}$ is the exact molecular energy in the adiabatic approximation.

The use of the Born-Oppenheimer product is motivated by the assumption that there is a lack of dynamical (non-adiabatic) coupling between the electron and the nuclei. This also implies that there is no such coupling in the target.

In Eq. (2.4.7) we have a wave function, consistent with the adiabatic-nuclei approximation, where the electronic part is given by the fixed-nuclei function that describes the electron-molecule scattering process in the fixed-nuclei framework. For this scattering process, the incoming electron will not contribute to the potential affecting the nuclei. The reason for this is the limited time the electron is present in the vicinity of the nuclei. This implies that $F_{n_i\nu_i J_i}(R)$ is the rovibrational wave function of the target's initial state [9].

Knowing the expression for the total wave function enables us to determine the total scattering amplitude [9]

$$T_{n_f\nu_f J_f, n_i\nu_i J_i}(\Omega' \Omega) = \int d\mathbf{R} F_{n_f\nu_f J_f}^*(\mathbf{R}) t_{n_f n_i}(\Omega', \Omega; \mathbf{R}) F_{n_i\nu_i J_i}(\mathbf{R}) \left(\frac{k_f}{k_{n_f}} \right) e^{i(k_{n_f} - k_f)r}. \quad (2.4.9)$$

Here k_{n_f} and k_{n_i} are the fixed-nuclei momenta of the final and initial states, respectively and they are related by Eq. (2.4.6), where $k_{n_i} \equiv k_i$ [9]. The direction of the incident and final momentum vectors, k_i and k_f , is specified by Ω and Ω' .

There are some concerns with formulating the total scattering amplitude as in Eq (2.4.9). In order for the calculated scattering amplitude to have a physical relevance, we must have a system where the approximation we have made truly is valid. Such a system would require that the fixed-nuclei momenta and the total momenta of the final states are almost equal,

$$k_f \approx k_{n_f}, \quad (2.4.10)$$

and that the potential energy curves of final and initial states are parallel in the Franck-Condon region, *i.e.* in the region where the initial vibrational wave function of the target molecule is non-zero [9]. These conditions apply for a system where the energy of the incoming electron is sufficiently higher than the excitation threshold and we get

$$\boxed{T_{n_f\nu_f J_f, n_i\nu_i J_i}(\Omega' \Omega) = \int d\mathbf{R} F_{n_f\nu_f J_f}(\mathbf{R}) t_{n_f n_i}(\Omega', \Omega; \mathbf{R}) F_{n_i\nu_i J_i}(\mathbf{R})}. \quad (2.4.11)$$

Thus, for systems where the impact energy is higher than the excitation threshold, the T -matrix elements can be obtained by averaging the fixed-nuclei amplitude over the initial and final ro-vibrational wave functions [9].

Up to this point, the electron scattering process has been considered *on* the energy shell. However, for reasons soon to be apparent, it is also common to evaluate the scattering amplitude *off* the energy shell.

When the electron scattering is calculated off the energy shell, we have that $k_f \neq k_{n_f}$ and $\varepsilon' \neq \varepsilon$, *i.e.* the initial and final energy of the scattered electrons are not the same [9].

Due to the restrictions mentioned earlier, the on-shell T -matrix fails to describe the electron scattering process near the excitation threshold. Therefore, an improved formulation of the scattering amplitude evaluated off the energy shell was also suggested by Shugard and Hazi,

$$T_{n_f\nu_f J_f, n_i\nu_i J_i}(\Omega'\Omega) = \int d\mathbf{R} F_{n_f\nu_f J_f}(\mathbf{R}) t_{n_f n_i}(\varepsilon'\Omega', \varepsilon\Omega; \mathbf{R}) F_{n_i\nu_i J_i}(\mathbf{R}). \quad (2.4.12)$$

Here, the T -matrix has been expressed off-shell with the energy ε defined as in Eq. (2.4.5) and ε' given as

$$\varepsilon' = \varepsilon_{n_f}(\mathbf{R}) + \frac{1}{2}k_f^2. \quad (2.4.13)$$

Here $t_{n_f n_i}(\varepsilon'\Omega', \varepsilon\Omega; \mathbf{R})$ is the fixed-nuclei scattering amplitude expressed off the energy shell. In the case where the impact energy is greater than the excitation threshold, the off-shell quantities are the same as their corresponding on-shell forms.

The off-shell formulation should give better results for systems where the scattering process occurs close to the excitation threshold as the off-shell k_f does not have to be restricted by Eq. (2.4.10). However, the off-shell $t_{n_f n_i}$ must be calculated separately for each ro-vibrational state, as the quantum numbers $(n_f\nu_f J_f)$ are needed to determine the magnitude of k_f .

2.5 Complex Kohn variational method

The fixed-nuclei electron scattering calculations were performed using an algebraic variational technique called the *Complex Kohn variational method* (CKVM) [10]. A trial wave function is created and inserted into a functional which, in turn, is minimized with respect to certain parameters. The basic approach of the CKVM for scattering of an electron-ion system with a spherically symmetric, short-range potential $V(r)$ will now be illustrated [10]. The partial wave radial Schrödinger equation can be given in the following manner

$$L\Phi_\ell = 0, \quad (2.5.1)$$

where L is given by

$$L = \left[-\frac{1}{2} \frac{d^2}{dr^2} + \frac{\ell(\ell+1)}{2r^2} + \frac{Z}{r} + V(r) - \frac{k^2}{2} \right]. \quad (2.5.2)$$

A functional, commonly called the Kohn functional I , is defined as follows

$$I[\Phi_\ell] = \int_0^\infty \Phi_\ell(r) L \Phi_\ell(r) dr. \quad (2.5.3)$$

The functional $I[\Phi_\ell] = 0$ if Φ_ℓ represents the exact solution. If instead a trial function, $\Phi_\ell^t \neq \Phi_\ell$, is inserted in Eq. (2.5.3), the functional will differ from zero. It is assumed that the following boundary conditions will apply to Φ_ℓ :

$$\begin{aligned} \Phi_\ell(0) &= 0 \\ \Phi_\ell(r \rightarrow \infty) &\sim F_\ell(kr) + \lambda G_\ell(kr). \end{aligned} \quad (2.5.4)$$

The Coulomb functions F_ℓ and G_ℓ are linearly independent solutions of Eq. (2.5.1) for the case where $V(r) = 0$ and λ is a linear coefficient. In order to study how the functional, I , behaves when a trial function is inserted in Eq. (2.5.1), we first have to define the deviance of Φ_ℓ^t from the exact solution Φ_ℓ ,

$$\delta\Phi_\ell(r) \equiv \Phi_\ell^t(r) - \Phi_\ell(r). \quad (2.5.5)$$

$\delta\Phi_\ell(r)$ is called the residual and it applied to the following boundary conditions

$$\begin{aligned} \delta\Phi_\ell(0) &= 0 \\ \delta\Phi_\ell(r \rightarrow \infty) &\sim \lambda G_\ell(kr). \end{aligned} \quad (2.5.6)$$

If Eq. (2.5.5) is substituted into the Kohn functional the following result is obtained after some simplification [10]

$$\delta I = -\frac{k}{2} W \delta\lambda + \int_0^\infty \delta\Phi_\ell L \delta\Phi_\ell dr. \quad (2.5.7)$$

The Wronskian, W , is given by

$$W = F_\ell(r) \frac{d}{dr} G_\ell(r) - G_\ell(r) \frac{d}{dr} F_\ell(r) \quad (2.5.8)$$

and $\delta\lambda = \lambda - \lambda^t$, where λ^t is a variational parameter and λ is the exact value. For a more detailed derivation of Eq. (2.5.7) refer to *e.g* [10]. Eq. (2.5.7) is called the Kato identity and it approximates λ with a stationary principle in the following manner:

$$\lambda^s = \lambda^t + \frac{2}{kW} \int_0^\infty \Phi_\ell^t L \Phi_\ell^t dr. \quad (2.5.9)$$

Eq. (2.5.9) can be solved with a suitable trial wave function. Such a function could have the following form,

$$\Phi_\ell^t(r) = f_\ell(r) + \lambda^t g_\ell(r) + \sum_{i=1}^n c_i \phi_i \quad (2.5.10)$$

where ϕ_i are square-integrable (L^2) functions and the functions f_ℓ and g_ℓ have the form

$$\begin{aligned} f_\ell(r \rightarrow \infty) &\sim F_\ell(kr) \\ g_\ell(r \rightarrow \infty) &\sim G_\ell(kr). \end{aligned} \quad (2.5.11)$$

If the above conditions apply, then the coefficients λ^t and c_i can be determined by

$$\frac{\partial \lambda^s}{\partial c_i} = \frac{\partial \lambda^s}{\partial \lambda^t} = 0. \quad (2.5.12)$$

Then, if Eq. (2.5.10) is substituted into Eq. (2.5.9) and the derivative with respect to c_i is taken, the following expression is obtained

$$\int_0^\infty \phi_i L \Phi_\ell^t dr = 0, \quad i = 1, \dots, n. \quad (2.5.13)$$

A corresponding expression is obtained for λ^t as

$$\int_0^\infty g_\ell L \Phi_\ell^t dr = 0. \quad (2.5.14)$$

If the basis functions ϕ_i and g_ℓ are taken as a single set $\{\phi_i\}$ $i = 0, \dots, n$, where $\phi_0 \equiv g_\ell$ and the linear parameters $\{\lambda^t, c_1, \dots, c_n\}$ are denoted by a vector \mathbf{c} we get

$$\mathbf{c} = -\mathbf{M}^{-1}\mathbf{s}. \quad (2.5.15)$$

Here \mathbf{M} is a matrix constituted by the following elements

$$M_{ij} = \int_0^\infty \phi_i L \phi_j dr, \quad i, j = 0, \dots, n \quad (2.5.16)$$

and the vector \mathbf{s} is constituted by the elements

$$s_i = \int_0^\infty \phi_i L f_\ell dr, \quad i = 0, \dots, n. \quad (2.5.17)$$

Substitution of Eq. (2.5.15) into Eq. (2.5.9) yields the following expression for the stationary value λ_s

$$\lambda^s = \frac{2}{kW} \left[\int_0^\infty f_\ell L f_\ell dr - \mathbf{s} \mathbf{M}^{-1} \mathbf{s} \right]. \quad (2.5.18)$$

In the case where g_ℓ is an outgoing function $h_\ell^+(r)$, we get

$$h_\ell^+(r) = \frac{i[F_\ell(kr) - iG_\ell(kr)]}{\sqrt{k}} \quad (2.5.19)$$

where $W = -1/k$ and Eq. (2.5.18) provides the formulation of the T -matrix, $\lambda^s = T_\ell^s = e^{i\delta_\ell} \sin \delta_\ell$ [10]

$$T_\ell^s = -2 \left[\int_0^\infty f_\ell L f_\ell dr - \mathbf{sM}^{-1}\mathbf{s} \right]. \quad (2.5.20)$$

The method is named after the symmetric matrix \mathbf{M} which has become a complex and at real energies the inverse is in general nonsingular [13].

In the generalization of CKVM to electron-molecule scattering the calculations are performed using the fixed-nuclei approximation. A trial function for multi-channel electron scattering in this framework is expressed as follows [10]

$$\Phi_n = \sum_{n'} \mathcal{A}(\chi_{n'} F_{n'n}) + \Theta_n. \quad (2.5.21)$$

Here, the first sum includes all energetically open N -electron target states, χ_n and the orbital function of the scattered electron, $F_{n'n}$. The operator, \mathcal{A} , anti-symmetrizes $F_{n'n}$ into the target states. (n, n') represent the incident and final channels respectively. n' is used to label all the quantum numbers needed to describe the physical state of the composite system. The second term of Eq. (2.5.21) is constituted of a set of $(N + 1)$ CSF's ,

$$\Theta_n = \sum_K d_K^n \Theta_K, \quad (2.5.22)$$

which are orthogonal to the $\chi_{n'} F_{n'n}$ terms.

The orbital function of the scattered electron can be expanded further as [10]

$$F_{n'n} = \sum_i c_i^{n'n} \phi_i + \sum_{\ell m} [f_\ell^{n'}(k_{n'} r) \delta_{\ell\ell_0} \delta_{mm_0} \delta_{n'n} + T_{\ell\ell_0 m m_0}^{n'n} g_\ell^{n'}(k_{n'} r)] \frac{Y_{\ell m}(\hat{r})}{r}, \quad (2.5.23)$$

where ϕ_i is a set of L^2 functions, *i.e.* they are square-integrable, and $Y_{\ell m}$ is a spherical harmonic. $f_\ell^{n'}$ and $g_\ell^{n'}$ are the continuum wave functions describing the incoming and outgoing scattered electron. $k_{n'}$ is the energy conserved channel momenta, $k_{n'}^2/2 = E - E_{n'}$, where $E_{n'}$ is the energy of the target state molecule and E is the total energy. The T -matrix elements, $T_{\ell\ell_0 m m_0}^{n'n}$, are fundamental to the calculation of the cross section. They depend on the internuclear distance as well as the energy of the scattered electron, E . Here, the T -matrix elements are calculated *on* the energy shell.

2.6 Wave packet methods

It was seen in the Introduction that in DE the inelastic electron scattering will transfer the molecular ion from the ground state to an excited electronic state. The excited system will have a specific total energy depending on the electron scattering energy and the initial state of the target ion and the process is usually described time-*independently*. However, in order to easily incorporate quantum effects and follow the process in time, the full time-dependent Schrödinger equation has to be solved and the wave packets are the solutions. However, before introducing the definition of a wave packet it makes sense to first discuss why it needs to be constructed.

The time-dependent Schrödinger equation (TDSE) for the radial nuclear motion of a diatomic molecule is given by

$$i\frac{\partial}{\partial t}\Psi(\mathbf{R}, t) = H\Psi(\mathbf{R}, t), \quad (2.6.1)$$

where the nuclear Hamiltonian operator is defined as

$$H = T_N + U = -\frac{1}{2\mu}\frac{\partial^2}{\partial R^2} + U(R). \quad (2.6.2)$$

This Hamiltonian can be recognized as the *nuclear Hamiltonian* as it is, by part constituted, of the nuclear kinetic energy operator for a diatomic molecule (see Eq. (2.1.2)). Note that in order to obtain Eq. (2.6.2) the rotational part of T_N is neglected. The solution to Eq. (2.6.1) is the time-dependent wave function, $\Psi(R, t)$, which by using separation of variables, can be expressed in the product form

$$\Psi(R, t) = \psi(R)\phi(t). \quad (2.6.3)$$

Substituting Eq. (2.6.3) into Eq. (2.6.1) yields

$$i\frac{d\phi(t)}{dt}\psi(R) = -\frac{1}{2\mu}\frac{d^2\psi(R)}{dR^2}\phi(t) + U\psi(R)\phi(t). \quad (2.6.4)$$

Dividing Eq. (2.6.4) through with $\psi(R)\phi(t)$ gives

$$i\frac{1}{\phi(t)}\frac{d\phi(t)}{dt} = -\frac{1}{2\mu}\frac{1}{\psi(R)}\frac{d^2\psi(R)}{dR^2} + U. \quad (2.6.5)$$

For Eq. (2.6.5) to be valid, both the right-hand side and the left-hand side must be equal to a constant. This separation constant is commonly called E for reasons that will soon become clear. Eq. (2.6.5) can then be divided into two separable

equations in the following manner

$$\begin{aligned}
i\frac{d\phi(t)}{dt} &= E\phi(t) \\
-\frac{1}{2\mu}\frac{d^2\psi_E(R)}{dR^2} + U\psi_E(R) &= E\psi_E(R).
\end{aligned}
\tag{2.6.6}$$

The second equation of (2.6.6) we recognize as the time-*independent* Schrödinger equation for the nuclear motion.

The solution of the time-dependent equation of (2.6.6) is solved easily, with multiplication from both sides with dt followed by integration over t , to

$$\phi(t) = \phi_0 e^{-iEt}. \tag{2.6.7}$$

Following Eq. (2.6.3) the solution to the TDSE is given by

$$\Psi(R, t) = \psi_E(R) e^{-iEt}, \tag{2.6.8}$$

where the factor ϕ_0 can be included into $\psi_E(R)$. Commonly the time-*independent* solutions are normalized in such a way that

$$\int_{-\infty}^{\infty} |\Psi(R, t)|^2 dr = 1. \tag{2.6.9}$$

It is evident that Eq. (2.6.3) is time-dependent, however, the probability density $|\Psi(R, t)|^2$ is not,

$$|\Psi(R, t)|^2 = \Psi^* \Psi = \psi_E^*(R) e^{iEt} \psi_E(R) e^{-iEt} = |\psi_E(R)|^2. \tag{2.6.10}$$

If the probability density is not time-dependent, it implies that the probability of finding the system in a specific state is time-*independent*, *i.e.* $\Psi(R, t)$ is a stationary state. However, if Eq. (2.6.8) is taken as a *particular solution* of the TDSE and the general solution is given by a linear combination of several particular solution, we get for the simplest case that

$$\Psi(R, t) = a\psi_{E_1}(R) e^{-iE_1 t} + b\psi_{E_2}(R) e^{-iE_2 t}. \tag{2.6.11}$$

The probability density of Eq. (2.6.11) is given as follows

$$|\Psi(R, t)|^2 = |a|^2 |\psi_{E_1}(R)|^2 + |b|^2 |\psi_{E_2}(R)|^2 + 2\text{Re} \{ a^* b \psi_{E_1}^*(R) \psi_{E_2}(R) e^{-i(E_2 - E_1)t} \}. \tag{2.6.12}$$

The first two terms of Eq. (2.6.12) are independent of time, however, the third, which is the interference term of the two first, is time-dependent. Thus, we have a solution of the TDSE that exhibits time-dependence also for the probability density. The interference term of Eq. (2.6.12) is what is called a wave packet

- a wave packet is the superposition of states of different energies, which is required in order to get a solution that has time-dependence in the probability density and other observable quantities [17].

The *general solution* of the TDSE is given as

$$\Psi(R, t) = \sum_{n=1}^{\infty} a_n \psi_n(R) e^{-iE_n t}. \quad (2.6.13)$$

Eq. (2.6.13) applies when the system has bound potential, resulting in solutions that only exist at certain discrete energies. The energy range in which physically interesting solutions can be found is called the *spectrum*; *i.e.* Eq. (2.6.13) gives the solution in a discrete spectrum. If the system constitutes an unbound potential, the interesting solutions are found in a continuous energy interval, rather than at discrete energies. The wave function for systems like this is given by

$$\Psi(R, t) = \int_0^{\infty} a(E) \psi_E(R) e^{-iEt} dE. \quad (2.6.14)$$

Thus, the solution of the TDSE in a continuous spectrum is given by Eq. (2.6.14).

When we know why it is needed, it makes sense to derive an actual wave packet. The simplest TDSE is the given for the free particle and the Hamiltonian for this system is defined as

$$H = -\frac{1}{2\mu} \frac{\partial^2 R}{\partial R^2}, \quad (2.6.15)$$

where the potential function is independent of the position and is taken as $U(R) = 0$. The time-*independent* solution is given as

$$\psi_E(R) = e^{\pm ikR}, \quad (2.6.16)$$

with the energy eigenvalues E forming a continuous spectrum

$$E = \frac{k^2}{2\mu} = \frac{p^2}{2\mu}. \quad (2.6.17)$$

By Eq. (2.6.8) a time-dependent particular solution to the TDSE is obtained as

$$\Psi(R, t) = e^{ikR} e^{-iEt} = e^{i(kR - \frac{k^2}{2\mu}t)}, \quad (2.6.18)$$

where k goes from $-\infty$ to ∞ . Substituting Eq. (2.6.18) into Eq. (2.6.14) we get the solution in the continuous spectrum

$$\Psi(R, t) = \int_{-\infty}^{\infty} a(k) e^{i(kR - \frac{k^2}{2\mu}t)} dk. \quad (2.6.19)$$

The initial condition of the wave packet, *i.e.* for $t = 0$, can easily be determined from Eq. (2.6.19),

$$\Psi(R, 0) = \int_{-\infty}^{\infty} a(k)e^{ikR}dk. \quad (2.6.20)$$

To determine the function $a(k)$ it is convenient to use Fourier transformation, Appendix I. Eq. (2.6.20) can be rewritten as a Fourier transformation by multiplication of both sides by $e^{-ik'R}$ and integrating over R . Using the Dirac delta function (Appendix I) we get

$$a(k) = \frac{1}{2\pi} \int_{-\infty}^{\infty} \Psi(R, 0)e^{-ikR}dR. \quad (2.6.21)$$

Thus, $\Psi(R, 0)$ and $a(k)$ are a Fourier pair. The same applies for the general solution

$$\Psi(R, t) = \int_{-\infty}^{\infty} a(k, t)e^{ikR}dk \quad (2.6.22)$$

when the function $a(k, t)$ is defined as follows

$$a(k, t) = a(k)e^{-i\frac{k^2}{2\mu}t}. \quad (2.6.23)$$

Similarly for $a(k, t)$ we get

$$a(k, t) = \frac{1}{2\pi} \int_{-\infty}^{\infty} \Psi(R, t)e^{-ikR}dR, \quad (2.6.24)$$

making $\Psi(R, t)$ and $a(k, t)$ another Fourier pair.

3 Derivation of cross section

With the theoretical background gained in section 2, we can now continue on to the cross section. In this section a time-dependent expression of the cross section of DE is derived from the more common time-independent form. With the time-dependent method, wave packet propagation is used to compute the cross section of dissociative excitation. A similar approach has been used to obtain the cross section of photodissociation.

This section begins with a short description of the work performed on photodissociation.

3.1 Cross section of photodissociation

Photodissociation is the process wherein a molecule is excited from the ground electronic state to an excited electronic state by absorption of a photon. The molecule then dissociates, either directly, or in a delayed fashion, depending on the nature of the potential of the excited state. Molecular processes like photodissociation can be studied using wave packets, a method that was seen early in the work of E. Heller in the 1970s [15, 16].

A property called the total absorption cross section σ , which provides a measure of the amount of light, with energy ω (atomic units), that can be absorbed by the system, can be used to study the photodissociation process. The cross section can be formulated time-*independently* or time-*dependently*. The derivation from a time-*independent* description to a time-*dependent* will now be given.

The total cross section of photodissociation can be defined in the following manner [15],

$$\sigma(\omega) \propto \omega |\langle \psi^-(E) | \mu_{td} | \chi_i \rangle|^2 \equiv \omega \Sigma(\omega), \quad (3.1.1)$$

Here $\psi^-(E)$ is the energy-normalized scattering eigenstate with the energy $E = E_i + \omega$. Furthermore, $|\chi_i\rangle$ is the initial vibrational state and μ_{td} is the transition dipole matrix element connecting the initial and final electronic states³. An alternative expression of Σ can also be obtained by

$$\Sigma(\omega) = \langle \phi | \psi^-(E) \rangle \langle \psi^-(E) | \phi \rangle \quad (3.1.2)$$

where $|\phi\rangle \equiv \mu_{td} |\chi_i\rangle$. The outgoing scattering states form a complete basis, *i.e.*

$$\mathbf{1} = \int |\psi^-(E')\rangle \langle \psi^-(E')| dE'. \quad (3.1.3)$$

³The elements of the transition dipole matrix are give by $\mu_{td} = \langle \phi_f | \hat{\mu} | \phi_i \rangle$.

Thus $\{\psi^-(E')\}$ can be rewritten using the Dirac delta function in the following manner,

$$\delta(E - H) = \delta(E - H) \cdot \mathbf{1} = |\psi^-(E)\rangle\langle\psi^-(E)|, \quad (3.1.4)$$

where H is the full Hamiltonian of the excited state. Substituting Eq. (3.1.4) into Eq. (3.1.2) yields

$$\Sigma(\omega) = \langle\phi|\delta(E - H)|\phi\rangle = \text{Tr}\{\delta(E - H)|\phi\rangle\langle\phi|\}. \quad (3.1.5)$$

Remembering that the Fourier transform of the Dirac-delta function is given by (see Appendix I subsection A.2)

$$\delta(E - H) = \frac{1}{2\pi} \int_{-\infty}^{\infty} e^{it(E-H)} dt, \quad (3.1.6)$$

$\Sigma(\omega)$ can be expressed in the following manner

$$\begin{aligned} \Sigma(\omega) &= \frac{1}{2\pi} \int_{-\infty}^{\infty} \langle\phi|e^{it(E-H)}|\phi\rangle dt = \frac{1}{2\pi} \int_{-\infty}^{\infty} e^{iEt} \langle\phi|e^{-iHt}|\phi\rangle dt \\ &= \frac{1}{2\pi} \int_{-\infty}^{\infty} e^{iEt} \langle\phi(0)|\phi(t)\rangle dt, \end{aligned} \quad (3.1.7)$$

where $\phi(t)$ is defined as follows

$$\phi(t) = e^{-iHt}|\phi\rangle. \quad (3.1.8)$$

From Eq. (3.1.7) it is evident that

the total photodissociation cross section is proportional to the Fourier transform of the overlap of the initial wave function $\phi(0)$ and the wave function when it has been propagated on the energy surface of the excited state [15].

An alternative formulation is that the Fourier transform of the autocorrelation of a wave packet propagated on the potential energy surface is the total cross section.

With the total cross section defined according to Eq. (3.1.7), it can further be shown that $|A(t)|$ is even around $t = 0$, where $A(t) \equiv \langle\phi(0)|\phi(t)\rangle$ is defined to be the correlation function [16]. Using Eq. (3.1.8) it is straight forward to show that

$$A^*(t) = A(-t). \quad (3.1.9)$$

From Eq. (3.1.9) it follows that $\Sigma(\omega)$ is real [16].

More details of the autocorrelation function can be found in Appendix I subsection A.3.

3.2 Cross section of dissociative excitation

For direct dissociative excitation it is common to calculate the cross section time-*independently* and for HeH⁺ there are both experimental [3, 4] and theoretical results [2]. Specifically, the formula for calculating the total fixed-nuclei excitation cross section of direct dissociative excitation time-*independently*, obtained from the work of Orel *et al.*, Eq. (1.2.1), was presented in the Introduction. In this section, we will make a somewhat extended description of this expression.

Further, we will also derive a time-dependent expression for calculating the cross section.

3.2.1 Derivation of delta-function approximation

In the work Orel *et al.* [2] a time-independent expression for a total cross section was derived by means of a delta-function approximation and using the fixed-nuclei excitation cross sections. We will now give a more detailed description of this expression.

In the complex Kohn variational method, the fixed-nuclei excitation cross sections are given by [2]

$$\tilde{\sigma}_{nn'}^{\Lambda}(E, R) = \frac{2\pi}{E} \sum_{\ell_0 \ell m_0 m} |T_{\ell_0 \ell m_0 m}^{\Lambda, nn'}(E, R)|^2. \quad (3.2.1)$$

Here $T_{\ell_0 \ell m_0 m}^{\Lambda, nn'}(E, R)$ is the fixed nuclei T-matrix on the energy shell.

We will use the work of Heller [15] on photodissociation (*see* also subsection 3.1) as a reference and firstly assume that a time-independent expression for the excitation cross section of DE can be formed by applying the adiabatic-nuclei approximation (compare to Eq. (3.1.1) and the adiabatic-nuclei definition of the on-shell T-matrix, Eq. (2.4.11)),

$$\sigma_{nn'}^{\Lambda}(E) \approx \frac{2\pi}{E} \sum_{\ell_0 \ell m_0 m} \int_{E_0}^E |\langle \psi_{E'}(R) | T_{\ell_0 \ell m_0 m}^{\Lambda, nn'}(E, R) | \chi_{\nu_0}(R) \rangle|^2 dE'. \quad (3.2.2)$$

Here $\psi_{E'}$ is an energy-normalized continuum function. $\Lambda = A_1, A_2, B_1$ refers the overall symmetry of the scattering and $n, n' = 0, 1, 2$ are the electronic states of the target. In this work $0 \rightarrow 1$ and $0 \rightarrow 2$ scattering is studied. E refers to the scattering energy and E' is the energy of the dissociative nuclear state. Hence, the energy of the ejected electron is given by $E - E'$. E_0 is the asymptotic energy the repulsive potential energy curve. Further, we also approximate the energy-normalized continuum wave function with the Dirac-delta function,

$$\psi_{E'}(R) \approx \left(\sqrt{\frac{dU}{dR}} \Big|_{R_{E'}} \right)^{-1} \delta(R - R_{E'}), \quad (3.2.3)$$

where $U(R)$ is the potential energy curve excited ionic state and $R_{E'}$ is the classical turning point at energy E' . Inserting Eq. (3.2.3) into Eq. (3.2.2) yields

$$\sigma_{nn'}^\Lambda(E) \approx \frac{2\pi}{E} \int_{E_0}^E \left(\frac{dU}{dR} \Big|_{R_{E'}} \right)^{-1} \sum_{\ell_0 \ell m_0 m} |T_{\ell_0 \ell m_0 m}^{\Lambda, nn'}(E, R_{E'})|^2 [\chi_{\nu_0}(R_{E'})]^2 dE'. \quad (3.2.4)$$

Hence, we can write Eq. (3.2.4) as

$$\sigma_{nn'}^\Lambda(E) = \int_{E_0}^E \left(\frac{dU}{dR} \Big|_{R_{E'}} \right)^{-1} \tilde{\sigma}_{nn'}^\Lambda(E, R_{E'}) [\chi_{\nu_0}(R_{E'})]^2 dE'. \quad (3.2.5)$$

Making the following change of variables,

$$\begin{aligned} U(R_{E'}) &= E' \\ dE' &= \frac{dU}{dR_{E'}} dR_{E'}, \end{aligned} \quad (3.2.6)$$

yields the following expression

$$\sigma_{nn'}^\Lambda(E) = \int_{R_E}^{\infty} \tilde{\sigma}_{nn'}^\Lambda(E, R) [\chi_{\nu_0}(R)]^2 dR. \quad \square \quad (3.2.7)$$

From Eq. (3.2.7) we see that the total fixed-nuclei excitation cross section is multiplied with the square of the vibrational wave function of the initial state of the target and integrated over the internuclear distance, R . This is the formula used by Orel *et al.*⁴ in their previous study of direct dissociative excitation of HeH⁺ [2].

3.2.2 Derivation of a time-dependent method

We also wish to derive a time-dependent model for calculating the cross section of DE. Therefore, we will use the time-*independent* formulation given in Eq. (3.2.2) as a starting point of this derivation.

By expanding the integrand Eq. (3.2.2) becomes

$$\sigma_{nn'}^\Lambda(E) = \frac{2\pi}{E} \sum_{\ell_0 \ell m_0 m} \int_{E_0}^E \langle \chi_{\nu} | [T_{\ell_0 \ell m_0 m}^{\Lambda, nn'}(E, R)]^* | \psi_{E'} \rangle \langle \psi_{E'} | [T_{\ell_0 \ell m_0 m}^{\Lambda, nn'}(E, R)] | \chi_{\nu} \rangle dE'. \quad (3.2.8)$$

Further, assuming that the continuum functions form a complete basis we can write, similarly to Eq. (3.1.4),

$$| \psi_{E'} \rangle \langle \psi_{E'} | = \delta(E' - H) = \frac{1}{2\pi} \int_{-\infty}^{\infty} e^{it(E'-H)} dt. \quad (3.2.9)$$

⁴In the previous formula by Orel *et al.* the lower bound of the integral was not $R_{E'}$ but a small internuclear distance for which the vibrational wave function is close to zero. This, however, has small influence on the final result.

Substituting Eq. (3.2.9) into Eq. (3.2.8) yields

$$\sigma_{nn'}^\Lambda(E) = \frac{2\pi}{E} \sum_{\ell_0 \ell m_0 m} \int_{E_0}^E \langle \chi_\nu | [T_{\ell_0 \ell m_0 m}^{\Lambda, nn'}(E, R)]^* e^{it(E'-H)} [T_{\ell_0 \ell m_0 m}^{\Lambda, nn'}(E, R)] | \chi_\nu \rangle dt dE' \quad (3.2.10)$$

Eq. (3.2.10) is time-dependent and the solution can be described with a wave packet (*see* subsection 2.6). The wave packet has the following initial condition,

$$\Psi_{\ell_0 \ell m_0 m}^{\Lambda, nn'}(E, t=0, R) = T_{\ell_0 \ell m_0 m}^{\Lambda, nn'}(E, R) \chi_\nu(R) \quad (3.2.11)$$

Upon substitution of Eq. (3.2.11) into Eq. (3.2.10) the following expression is obtained

$$\sigma_{nn'}^\Lambda(E) = \frac{2\pi}{E} \frac{1}{2\pi} \sum_{\ell_0 \ell m_0 m} \int_{E_0}^E \int_{-\infty}^{\infty} e^{iE't} \langle \Psi_{\ell_0 \ell m_0 m}^{\Lambda, nn'}(E, 0, R) | e^{-iHt} \Psi_{\ell_0 \ell m_0 m}^{\Lambda, nn'}(E, 0, R) \rangle dt dE', \quad (3.2.12)$$

where we have that

$$\Psi_{i,j}^{\Lambda, nn'}(E, t, R) = e^{-iHt} \Psi_{\ell_0 \ell m_0 m}^{\Lambda, nn'}(E, 0, R). \quad (3.2.13)$$

The autocorrelation function can be formed as

$$A_{\ell_0 \ell m_0 m}^{\Lambda, nn'}(E, t) = \langle \Psi_{\ell_0 \ell m_0 m}^{\Lambda, nn'}(E, 0, R) | \Psi_{\ell_0 \ell m_0 m}^{\Lambda, nn'}(E, t, R) \rangle. \quad (3.2.14)$$

Eqs. (3.2.13) and (3.2.14) are substituted into Eq. (3.2.12) and we note that upon application of the inverse Fourier operator on the integrand yields

$$\frac{1}{2\pi} \int_{-\infty}^{\infty} e^{iE't} A_{\ell_0 \ell m_0 m}^{\Lambda, nn'}(E, t) dt = \mathcal{F}^{-1} \{ A_{\ell_0 \ell m_0 m}^{\Lambda, nn'}(E, t) \} = a_{\ell_0 \ell m_0 m}^{\Lambda, nn'}(E, E'). \quad (3.2.15)$$

The time-dependent expression for the cross section is thus given as

$$\sigma_{nn'}^\Lambda(E) = \frac{2\pi}{E} \sum_{\ell_0 \ell m_0 m} \int_{E_0}^E a_{\ell_0 \ell m_0 m}^{\Lambda, nn'}(E, E') dE', \quad (3.2.16)$$

and the total cross section is obtained by summation over all symmetries,

$$\sigma_{nn'}(E) = \sigma_{nn'}^{A_1}(E) + \sigma_{nn'}^{A_2}(E) + 2\sigma_{nn'}^{B_1}(E). \quad (3.2.17)$$

We thus obtain

$$\boxed{\sigma_{nn'}^\Lambda(E) = \frac{2\pi}{E} \frac{1}{2\pi} \sum_{\ell_0 \ell m_0 m} \int_{E_0}^E \int_{-\infty}^{\infty} e^{iE't} \langle \Psi_{\ell_0 \ell m_0 m}^{\Lambda, nn'}(E, 0, R) | \Psi_{\ell_0 \ell m_0 m}^{\Lambda, nn'}(E, t, R) \rangle dt dE'}. \quad (3.2.18)$$

This is the time-dependent method that will be implemented and tested in the present study of direct DE of HeH⁺.

4 Computational Details

In this section computational details on the electronic structure calculations and electron scattering calculations that form the input for the calculation of the cross section will be given. The choice of symmetry in which these calculations are performed will also be briefly explained.

Further, the implementation of the time-independent and time-dependent expressions for calculating the cross section of DE, as given in subsection 3.2, will be described. We will implement two methods for calculating a the cross section time-independently; the fixed-nuclei cross section averaged over the initial vibrational wave function [Eq. (3.2.7)] (the delta-function approximation), as well as the cross section obtained by projection on energy-normalized continuum wave functions [Eq. (3.2.2)]. And one time-dependent wave packet method [Eq. (3.2.18)] will be tested.

4.1 A note on symmetry

It is common to characterize a molecule by its symmetry. Which symmetry group (point group) a molecule belongs is determined by how it is affected by symmetry operations such as rotation around different axes, reflection in mirror planes *etc.* Thus, in order to decide which point group a molecule belong to, the symmetry elements of the structures have to be decided. The easiest way to assign the correct point group to a molecule is to follow a common 'yes-no' table⁵.

The symmetry operations of each point group can be described by the *irreducible representations*. The irreducible representation "+1/ - 1" this means that the symmetry operation is symmetric/antisymmetric. Each set of irreducible representations corresponds to an overall symmetry, such as A_1, A_2, B_1 , *etc.* The irreducible representations of the C_{2v} point group is displayed in table 4.1.1.

Table 4.1.1: Irreducible representations for a molecule of C_{2v} symmetry. C_2 denotes the principal rotation axis and σ the two mirror planes.

C_{2v}	E	$C_2(z)$	$\sigma_v(xz)$	$\sigma_v(yz)$
A_1	1	1	1	1
A_2	1	1	-1	-1
B_1	1	-1	1	-1
B_2	1	-1	-1	1

⁵Such as the one present on page 167 in Kettle, S. F. A., *Symmetry and Structure*, (Wiley, New York, 1985).

The HeH^+ molecule is linear and does not have inversion symmetry. This means that we should assign it the $C_{\infty v}$ point group. However, this means that the HeH^+ molecule has an infinite number of irreducible representations. Therefore, we have assigned the molecule the C_{2v} point group for all computational purposes. Thus there will be four possible symmetries; A_1, A_2, B_1 and B_2 . The Σ^+ in $C_{\infty v}$ symmetry corresponds A_1 symmetry, the Σ^- corresponds to A_2 . The two components of the Π -states will fall into the the B_1 and B_2 symmetries, while the two components of the Δ -states will go into A_1 and A_2 *etc.*. Since B_1 and B_2 will give identical contribution we only need to calculate one of them and include it twice in the final result.

4.2 Structure calculations

The electronic structure calculations were performed using the aug-cc-pVQZ [19] basis set for He and the aug-cc-pVTZ [20] basis set for H. One extra diffuse d-functions was also added on He, resulting in a total of 106 functions.

Using these basis sets a SCF calculation on the ionic ground state was performed. Then a full CI calculation was performed on the three lowest excited states of the ion. From the full CI, natural orbitals are computed.

All the possible excitations of the three electrons within the ten lowest natural orbitals form the reference configurations for the MRCI calculation. Additional single external excitations are also included.

4.3 Electron scattering calculations

The electron scattering calculations, using CKVM [10], are performed in A_1, A_2 and B_1 symmetries, using the same target wave functions as the ones used in the MRCI calculations. Scattering is calculated at the following internuclear distances R (in a_0):

$$R = 1.0, 1.1, 1.2, 1.25, 1.3, 1.35, 1.4, 1.45, 1.5 \\ 1.55, 1.6, 1.7, 1.8, 1.9, 2.0, 2.1, 2.2, 2.3, \\ 2.4, 2.5, 2.6, 2.7, 2.8, 3.0, 3.2, 3.4, 3.6, 3.8.$$

The energy interval of the scattering calculations is spanning from 15 eV to 38.9 eV in steps of 0.1 eV.

From each calculation the total fixed-nuclei elastic and inelastic scattering cross sections, T -matrices *etc.* are obtained. The size of the T -matrices are connected to the number of open channels, *i.e* the energy, and the number of (ℓ, m) -pairs that are included in the calculation. If N (ℓ, m) -pairs are included in the calculation, and only one channel is open, then the size of the T -matrix is $N \times N$. For higher

energies, when two or three channels are open, the size of the T-matrix will double and triple, respectively.

The electron scattering calculations for the respective symmetries were performed for the following (ℓ, m) -pairs:

$$A_1 : (\ell, m) = (0, 0), (1, 0), (2, 0), (3, 0), (4, 0) \\ (5, 0), (6, 0), (2, -2), (3, -2), (4, -2) \\ (5, -2), (6, -2), (4, -4), (5, -4), (6, -4)$$

$$A_2 : (\ell, m) = (2, 2), (3, 2), (4, 2), (5, 2), (6, 2)$$

$$B_1 : (\ell, m) = (1, -1), (2, -1), (3, -1), (3, -3) \\ (4, -1), (4, -3), (5, -1), (5, -3), (6, -1) \\ (6, -3)$$

Thus, in the present study scattering with partial wave with $\ell \leq 6$, $|m| \leq 4$ are included.

4.4 Wave packet calculations

In the time-dependent expression for the cross section of DE, wave packet propagation is used, as described by Eq. (3.2.18). The initial condition made up of the $v = 0$ vibrational wave function and a T-matrix element [see Eq. (3.2.11)].

As the purpose is to test if the cross section of the DE of HeH^+ can be calculated using our suggested time-dependent model, this calculation will be performed only for a simple model system where the the two first T-matrix elements in B_1 symmetry for the $X^1\Sigma^+ \rightarrow a^3\Sigma^+$ transition are included. This result will be an indication of the feasibility of the model.

The parameters giving the best convergence are $dr = 0.01$ and $dt = 0.12$ (see Appendix II - Convergence testing of the wave packet model). The wave packet is then propagated for 3000 time steps, using a propagation method based on the *Crank-Nicholson* method [18].

4.5 Time-independent calculations

As there is a previous theoretical result [2] of the cross section of HeH^+ obtained time-independently, it is meaningful to compute this quantity and compare the results. It is also interesting to compare the different approaches to calculate the time-independent cross section. Within the scope of this project we have chosen to implement two different methods to compute the cross section of DE time-independently.

The expression given by Eq. (3.2.7) will give a total cross section averaged over the initial vibrational wave function. It was presented in the work of Orel *et al.* and here the fixed-nuclei excitation cross sections, calculated according to Eq. (3.2.1), are used. In this method we have to make the delta-function approximation described in subsection 3.2. Nevertheless, as the fixed-nuclei excitation cross sections are available from the scattering calculation output, this method has the advantage that we do not have to use the T-matrix elements directly. This greatly reduces the amount of data that has to be used in the calculation. Therefore, we can obtain the total time-independent cross section according to Eq. (3.2.17).

This method will also be implemented using only the first two T-matrix elements in B_1 symmetry. Thus obtaining a partial cross section only for these two elements. We do this in order to compare with the cross section obtained time-dependently.

An alternative way, is to use Eq. (3.2.2), where the cross section is obtained by projection on the energy-normalized continuum wave functions [Eq. (3.2.3)]. Here, the individual T-matrix elements are also used directly, however, because of the projection on the eigenstates of the continuum wave function it means we avoid making a delta-function approximation. Using this method, we will calculate a partial the cross section in B_1 symmetry, and compare this result with the result obtained from the time-dependent model.

5 Results

5.1 Fixed-nuclei cross section

In order to calculate the total cross section using Eq. (3.2.7), the fixed-nuclei inelastic excitation cross section for a certain internuclear distance, $\tilde{\sigma}_{nn'}^{\Lambda}(E, R)$ is needed. $\tilde{\sigma}_{nn'}^{\Lambda}(E, R)$ is computed for the complete E -grid for each R and the result at $1.45 a_0$ (near equilibrium distance) for A_1 symmetry is displayed in Fig. 7.

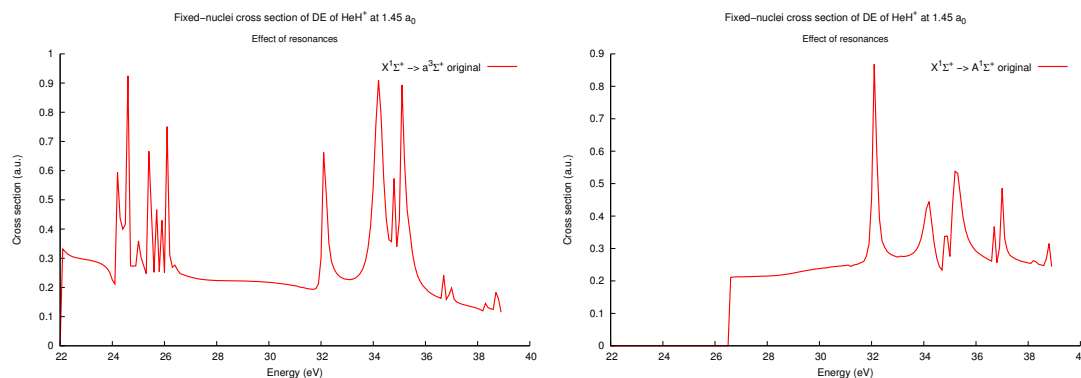


Figure 7: The fixed-nuclei cross section for A_1 symmetry at internuclear distance $1.45 a_0$. The fixed-nuclei cross section is clearly influenced by the resonance process. The $X^1\Sigma^+ \rightarrow a^3\Sigma^+$ transition is displayed to the left and the $X^1\Sigma^+ \rightarrow A^1\Sigma^+$ transition to the right. Observe that here the cross section is given in atomic units.

The peaks that can be seen in Fig. 7 are a result of the resonant process that is competing with the direct process. In order to obtain a cross section that only includes the direct DE, resonances are removed. The result of this treatment is shown for A_1 symmetry at $1.45 a_0$ in Fig. 8.

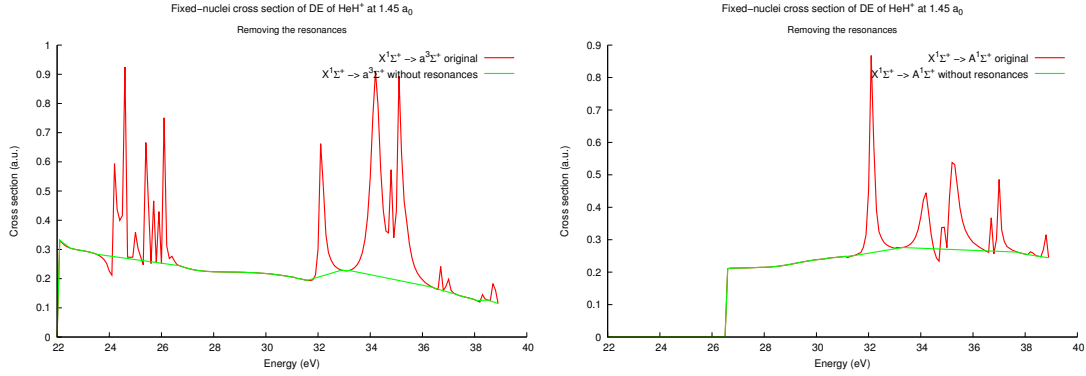


Figure 8: The resonances are removed and the result is spline onto the same R -grid as before. For A_1 symmetry at $1.45 a_0$, this treatment removes the resonance behavior. Observe that here the cross section is given in atomic units.

From Fig. 8 we can see that when the resonances are removed the cross section quite smoothly follows the background. This procedure is repeated for all R and symmetries. After this has been done we can calculate the averaged fixed-nuclei cross section can be calculated both with and without including the resonances. Thus we can see how much the total cross section is affected by the resonances. More details on the subject of resonances will be given in subsection 5.2.

5.2 Effect of resonances

Along with the direct DE there are occurring resonant processes in which the excited electron is temporarily captured into a Rydberg state from where it eventually autoionizes to $H + He^+$. (For low energies, *Resonant dissociative excitation* where the system autoionizes to $He + H^+$ can also occur.) Fig. 9 illustrates the resonance behavior at high and low energies, respectively.

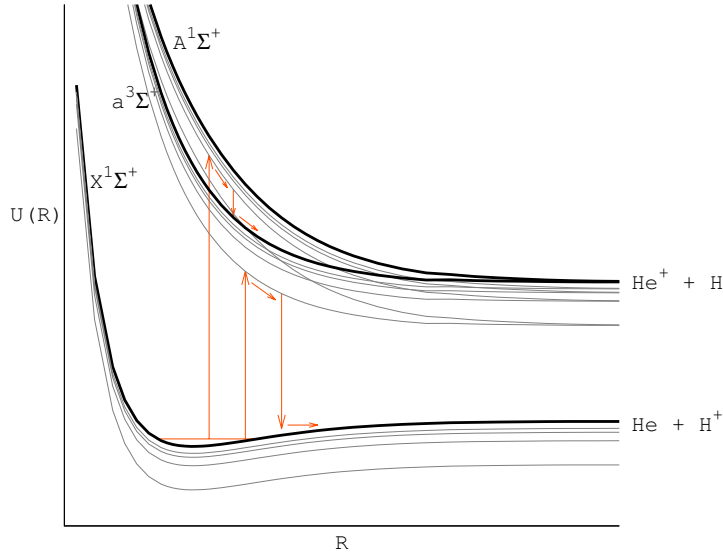


Figure 9: At low energies the the electron can be captured into one of the Rydberg states associated with the $a^3\Sigma^+$ state and the system autoionizes to $\text{He} + \text{H}^+$. At higher energies, the electron can be captured into a Rydberg state associated with the $A^1\Sigma^+$ state. This results in autoionization to $\text{He} + \text{H}^+$

The resonant process occurs naturally for electron scattering processes like DE. Thus, we would have to include both direct DE and resonant processes, as well as any interactions of the Rydberg states with the continuum, to exactly describe the full reaction mechanism.

The output of scattering calculations will include both the direct and the resonant process. However, in this project we are only focusing on the direct DE process and thus the contribution from the resonant states are removed. There are more and less sophisticated methods to deal with the resonances. Here, a somewhat "brute force" method, consisting of removing any data points in the scattering output where there are resonance behavior, is employed. The data set without the resonances are then splined onto the same R -grid as the original data.

5.3 Total cross section of DE obtained using the delta-function approximation

Using the fixed-nuclei excitation cross sections, $\tilde{\sigma}_{nn'}^\Lambda(E, R)$, calculated with the full T-matrix obtained from the complex Kohn variational method, we calculated an averaged fixed-nuclei cross section using Eq. (3.2.7) without removing the resonances. Upon averaging over the square of the initial vibrational wave function ($v = 0$) the result displayed in Fig. 10 was obtained.

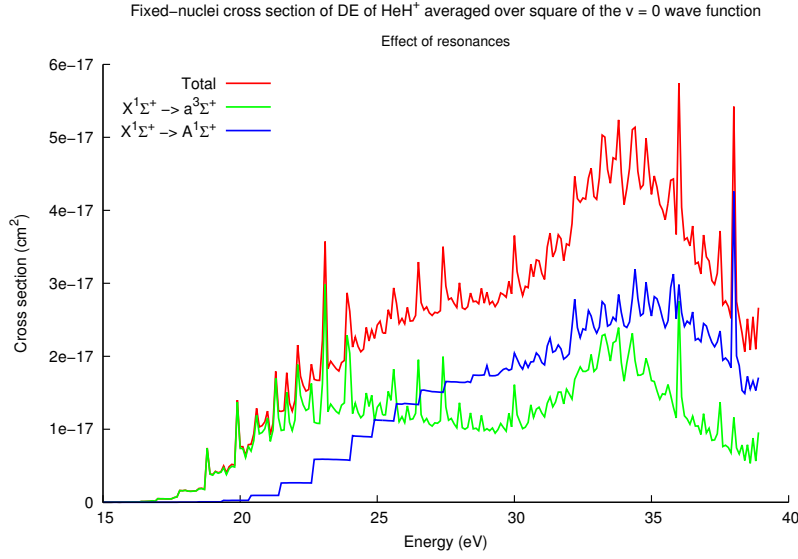


Figure 10: Total fixed-nuclei cross section averaged over the square of the initial vibrational wave function. The total is given as the sum of the cross section of the $X^1\Sigma^+ \rightarrow a^3\Sigma^+$ and $X^1\Sigma^+ \rightarrow A^1\Sigma^+$ transitions. The cross section suffers from clear resonance behavior.

Evidently there are sharp structures from the resonant states over the entire energy interval. Additionally there are clear jumps at the onset of the $X^1\Sigma^+ \rightarrow A^1\Sigma^+$ cross section. This clear definition of energy thresholds could possibly be remedied by carrying out the electron scattering calculations using a closer spacing on the internuclear distance grid. This is something that was not examined in this project. Instead, additional splining was used to remove this behavior.

The resonances were then removed and the splined data was averaged over the $v = 0$ vibrational wave function and the result displayed in Fig. 11 is obtained.

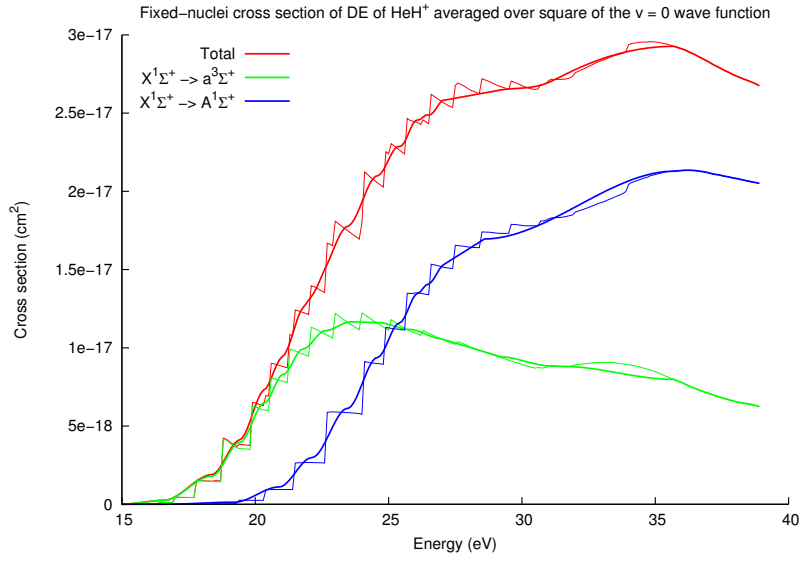


Figure 11: The removing of the resonances results in a much smoother total cross section. There are still some jumps in the cross section around the energy thresholds but we can clearly follow the trend of the total averaged fixed-nuclei cross section.

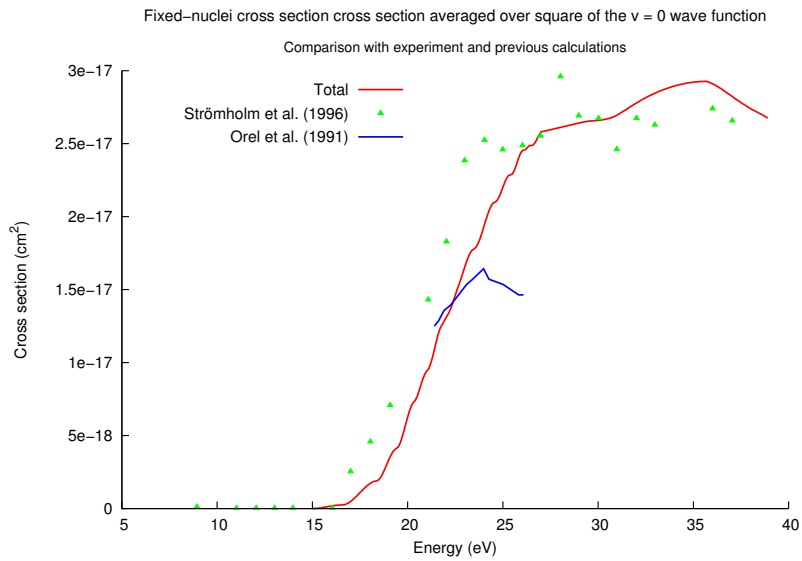


Figure 12: The total averaged cross section is compared with the experimental result of Strömholm *et al.* [4] and the theoretical result of Orel *et al.* [2]. Our computed result shows quite good agreement with the experiment.

The total cross section obtained in the above described manner is compared

with the experimental result of Strömholm *et al.* [4] in Fig 12. We can see that our theoretical result shows quite good agreement with the experimental result.

A partial cross section with only the two first T-matrix elements, was also computed for the $X^1\Sigma^+ \rightarrow a^3\Sigma^+$ transition in B_1 symmetry. The result is displayed in Fig. 13. This result will be compared with the more accurate cross section computed using the time-independent and time-dependent methods described above.

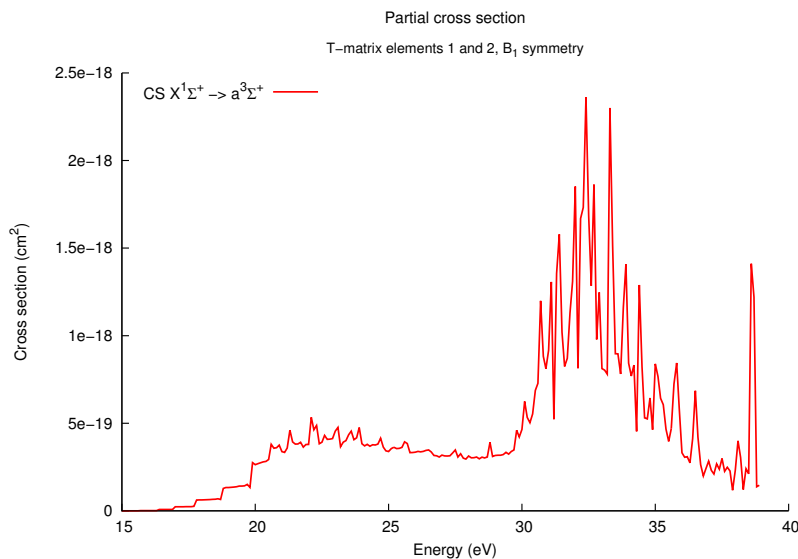


Figure 13: Partial cross section obtained using only specific T-matrix elements. Here T-matrix elements 1 and 2 in B_1 symmetry for the $X^1\Sigma^+ \rightarrow a^3\Sigma^+$ transition were included.

5.4 Time-independent cross section using the energy-normalized continuum functions

A time-independent cross section was also calculated with only the two first T-matrix elements for the $X^1\Sigma^+ \rightarrow a^3\Sigma^+$ transition in B_1 symmetry using Eq. (3.2.2). The result is displayed in Fig. 14.

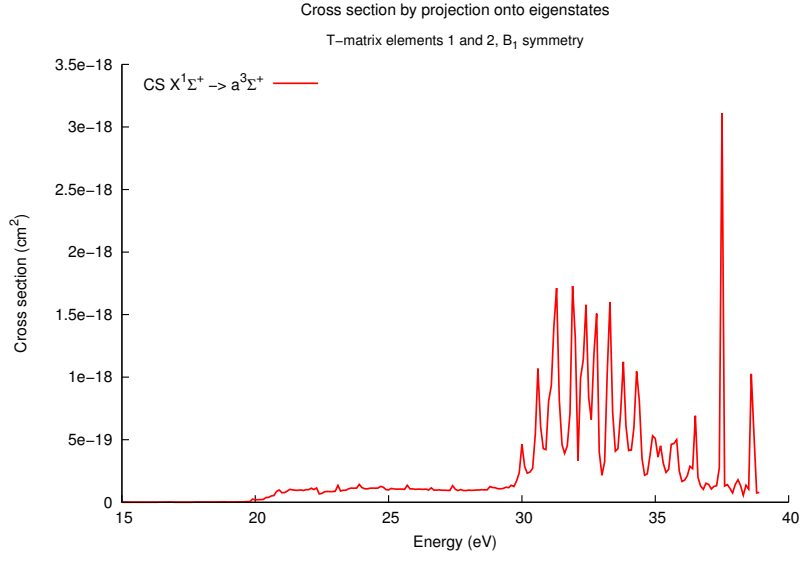


Figure 14: Cross section obtained by projection on the energy-normalized eigenfunctions [Eq. (3.2.2)]. Here T-matrix elements 1 and 2 in B_1 symmetry for the $X^1\Sigma^+ \rightarrow a^3\Sigma^+$ transition were included.

5.5 Time-dependent results

With the time-dependent wave packet method, a cross section was calculated using the first two T-matrix elements for the $X^1\Sigma^+ \rightarrow a^3\Sigma^+$ transition in B_1 symmetry. The result is displayed in Fig. 15.

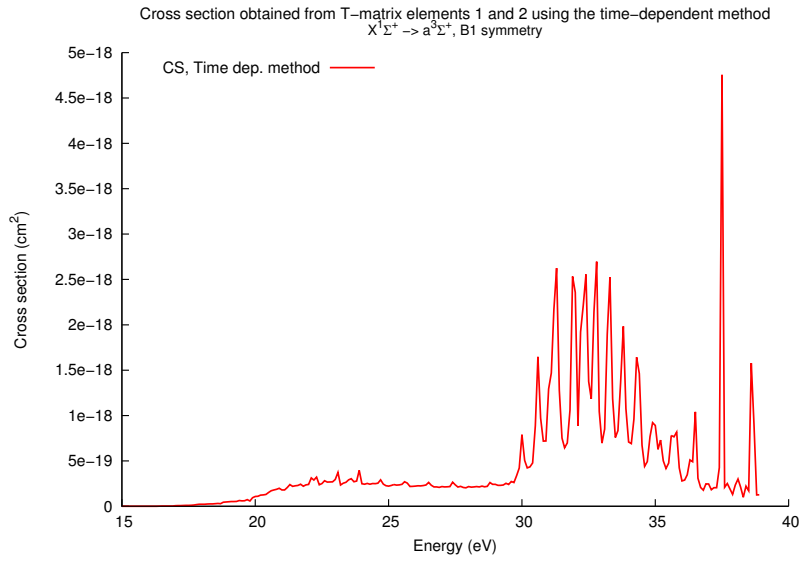


Figure 15: Time-dependent cross section obtained with wave packet method [Eq. (3.2.18)] for 3000 time steps. T-matrix elements 1 and 2 in B_1 symmetry for the $X^1\Sigma^+ \rightarrow a^3\Sigma^+$ transition were included.

5.6 Comparison of time-dependent and time-independent methods

The results of the time-independent calculations using the delta-function approximation and the projection on the energy-normalized continuum wave functions are compared with the results of the time-dependent method. The cross sections are displayed in Fig. 16

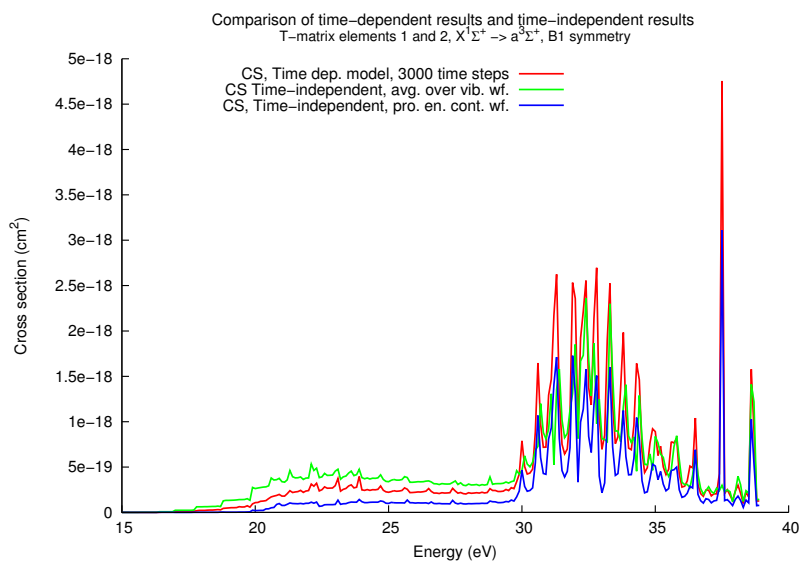


Figure 16: Comparison of the result using the time-dependent model and the cross sections obtained time-independently. Here, only T-matrix elements 1 and 2 in B_1 symmetry for the $X^1\Sigma^+ \rightarrow a^3\Sigma^+$ transition were used.

6 Discussion

7 Concluding Remarks

7.1 Further applications of method

A Appendix I

A.1 Fourier transformation

Fourier transformation is a useful tool when dealing with functions such as the *Delta function* and the *Autocorrelation function*. Therefore, it makes sense to introduce the Fourier transform before presenting the details of any these functions. The Fourier transform of the function $f(t)$ is defined in terms of the angular frequency, ω , in the following manner

$$\tilde{f}(\omega) = \int_{-\infty}^{\infty} f(t)e^{-i\omega t} dt. \quad (\text{A.1.1})$$

An abbreviated formulation using the *Fourier operator* is given as

$$\tilde{f}(\omega) = \mathcal{F}\{f(t)\}. \quad (\text{A.1.2})$$

For a function $f(t)$ fulfilling the condition of being piecewise continuous and rapidly decaying to 0 as $|t| \rightarrow \infty$ the Eq. A.1.1 is defined for all $\omega \in \mathbb{R}$. An *inverse Fourier transform*, i.e. moving from ω -space back to t -space, is defined as follows

$$f(t) = \frac{1}{2\pi} \int_{-\infty}^{\infty} \tilde{f}(\omega)e^{i\omega t} d\omega. \quad (\text{A.1.3})$$

Eq. (A.1.3) can also be expressed using the Fourier operator in the following manner

$$f(t) = \mathcal{F}^{-1}\{\tilde{f}(\omega)\}. \quad (\text{A.1.4})$$

An important property of the Fourier transform is the *Convolution theorem*. If the convolution integral is defined as

$$f * g = \int_{-\infty}^{\infty} f(t')g(t-t')dt', \quad (\text{A.1.5})$$

the Fourier transform of Eq. (A.1.5) is given as

$$\mathcal{F}\{f * g\} = \tilde{f}(\omega)\tilde{g}(\omega). \quad (\text{A.1.6})$$

In principle, taking the Fourier transform of the convolution integral is the same as taking the Fourier transform of the individual functions separately. The proof of the Convolution theorem will be presented after the delta function is introduced. From Eq. (A.1.6) the inverse transformation follows trivially. Making the variable substitution $\xi = t - t'$ it can be found that Eq. (A.1.5) is commutative.

$$\int_{-\infty}^{\infty} f(t' - \xi)g(\xi)d\xi = g * f \quad (\text{A.1.7})$$

Another useful feature of the Fourier transform is given by the *Fourier integral theorem*,

$$f(t') = \frac{1}{2\pi} \int_{-\infty}^{\infty} e^{-i\omega t'} d\omega \int_{-\infty}^{\infty} f(t)e^{i\omega t} dt. \quad (\text{A.1.8})$$

Eq. (A.1.8) is developed from the Fourier series and its derivation can be found e.g. in chapter 15 of *Arfken & Weber* [21].

A.2 The Dirac delta function

The Dirac delta function can be defined in a general manner by [22]

$$\int_{-\infty}^{\infty} f(t)\delta(t - t')dt = f(t') \quad (\text{A.2.1})$$

and

$$\int_{-\infty}^{\infty} \delta(t)dt = 1. \quad (\text{A.2.2})$$

In the case where $t' = 0$ Eq. (A.2.1) becomes

$$\int_{-\infty}^{\infty} f(t)\delta(t)dt = f(0). \quad (\text{A.2.3})$$

The Fourier transform of the delta function is very useful and it is used several times in this work. It is derived from the Fourier Integral (Eq. (A.1.8)) where the order of integration has been reversed leading to the following expression,

$$f(t') = \int_{-\infty}^{\infty} f(t) \left[\frac{1}{2\pi} \int_{-\infty}^{\infty} e^{i\omega(t-t')} d\omega \right] dt. \quad (\text{A.2.4})$$

Following the definition of the delta function, given in Eq. (A.2.1) it is trivial to see that,

$$\delta(t - t') = \frac{1}{2\pi} \int_{-\infty}^{\infty} e^{i\omega(t-t')} d\omega. \quad (\text{A.2.5})$$

For a more detailed derivation of Eq. (A.2.5) see e.g. chapter 15 *Arfken & Weber* [21].

The usefulness of the delta function will now be illustrated in the proof of the convolution theorem presented in Eq. (A.1.6) [17]. Starting by taking the inverse Fourier transform of RHS of Eq. (A.1.6) and expressing \tilde{f} and \tilde{g} also using the inverse Fourier transform the following expression is obtained

$$\mathcal{F}^{-1} \left\{ \tilde{f}(\omega) \tilde{g}(\omega) \right\} = \frac{1}{2\pi} \int_{-\infty}^{\infty} \left\{ \int_{-\infty}^{\infty} f(t') e^{i\omega t'} dt' \right\} \left\{ \int_{-\infty}^{\infty} g(t'') e^{i\omega t''} dt'' \right\} e^{i\omega t} d\omega. \quad (\text{A.2.6})$$

By rearranging the order of integration we get

$$\mathcal{F}^{-1} \left\{ \tilde{f}(\omega) \tilde{g}(\omega) \right\} = \int_{-\infty}^{\infty} \int_{-\infty}^{\infty} f(t') g(t'') \left(\frac{1}{2\pi} \int_{-\infty}^{\infty} e^{i\omega(t-(t'+t''))} d\omega \right) dt' dt''. \quad (\text{A.2.7})$$

Using Eq. (A.2.5) the following expression is obtained

$$\mathcal{F}^{-1} \left\{ \tilde{f}(\omega) \tilde{g}(\omega) \right\} = \int_{-\infty}^{\infty} \int_{-\infty}^{\infty} f(t') g(t'') \delta(t - (t' + t'')) dt' dt'', \quad (\text{A.2.8})$$

Thus by Eq. (A.2.1)

$$\mathcal{F}^{-1} \left\{ \tilde{f}(\omega) \tilde{g}(\omega) \right\} = \int_{-\infty}^{\infty} f(t') g(t - t') dt' \quad \square \quad (\text{A.2.9})$$

A.3 The autocorrelation function

The *autocorrelation* function, $A(t)$, is convenient to use due to its connection with the spectra of the wave packet $\sigma(\omega)$. The autocorrelation function is defined in the following manner

$$A(t) = \langle \Psi(0) | \Psi(t) \rangle, \quad (\text{A.3.1})$$

and it describes the overlap between the initial wave packet and the wave packet after a time t . By expressing the wave packet is given by the solutions for the bound state problem,

$$\Psi(x, t) = \sum_n c_n \psi_n(x) e^{-iE_n t}. \quad (\text{A.3.2})$$

The spectrum of the wave packet is defined as

$$\sigma(\omega) = \sum_n |c_n|^2 \delta(\omega - \omega_n), \quad (\text{A.3.3})$$

where $\omega_n = E_n$. The spectrum also can be obtained as the Fourier transform of the autocorrelation of the wave packet,

$$\sigma(\omega) = \frac{1}{2\pi} \int_{-\infty}^{\infty} A(t) e^{i\omega t} dt. \quad (\text{A.3.4})$$

This connection between the spectrum and the autocorrelation function can be proven in the following manner [17]:

$$\sigma(\omega) = \frac{1}{2\pi} \int_{-\infty}^{\infty} \langle \Psi(0) | \Psi(t) \rangle e^{i\omega t} dt \quad (\text{A.3.5})$$

By substituting Eq. (A.3.2) into Eq. (A.3.5) we obtain

$$\begin{aligned} \sigma(\omega) &= \frac{1}{2\pi} \int_{-\infty}^{\infty} \int_{-\infty}^{\infty} \left(\sum_m c_m^* \psi_m^*(x) \right) \left(\sum_m c_m e^{-iE_n t} \psi_n(x) \right) dx e^{i\omega t} dt \\ &= \frac{1}{2\pi} \int_{-\infty}^{\infty} \sum_{m,n} c_m^* c_n \delta_{mn} e^{-iE_n t} e^{i\omega t} dt \\ &= \frac{1}{2\pi} \sum_n |c_n|^2 \int_{-\infty}^{\infty} e^{-iE_n t} e^{i\omega t} dt = \{\text{using Eq. (A.2.5)}\} \\ &= \sum_n |c_n|^2 \delta(\omega - E_n) \\ &= \sum_n |c_n|^2 \delta(\omega - \omega_0) \quad \square \end{aligned} \quad (\text{A.3.6})$$

It can be proven that the autocorrelation of the wave packet and the photodissociation cross section, too, are connected through a Fourier transform (see Theory subsection 3.1).

B Appendix II - Convergence testing of the wave packet model

The quality of the result of the wave packet propagation will not only rely on the input from the scattering calculations, but it will also be dependent on the numerical stability of the calculations. One way to obtain numerically stable calculations is to test the convergence of the numerical variables. The numerical variables for which we have tested the convergence of the model are: the step size on the R-grid, dr , and the time step size, dt . dr and dt is tested prior to introduction of the T-matrix elements, using an higher order vibrational wave function ($v = 5$, as it was the most sensitive to the numerical instability). Now the results of the convergence testing will be summarized.

The results of the convergence testing of the autocorrelation function and the corresponding cross section (*i.e.* the Fourier transform of overlap of the $v = 5$ vibrational wave function and the propagated wave function) for variation of dt are presented in Fig. 17.

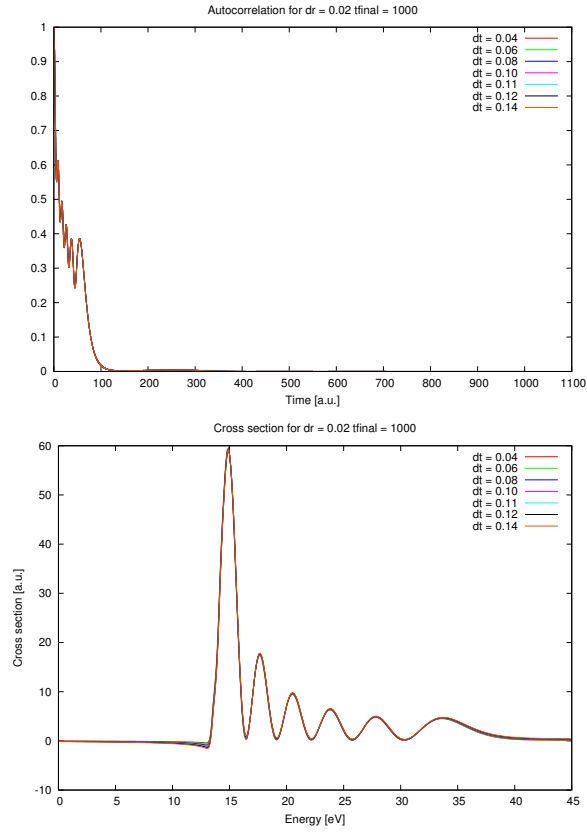


Figure 17: The autocorrelation and the cross section calculated for different dt . We can see that the result does not seem to be considerably affected by the choice of dt .

We notice that variation of dt does not affect the convergence of the autocorrelation and cross section substantially. Therefore, $dt = 0.12$ is deemed to be sufficient for our calculations.

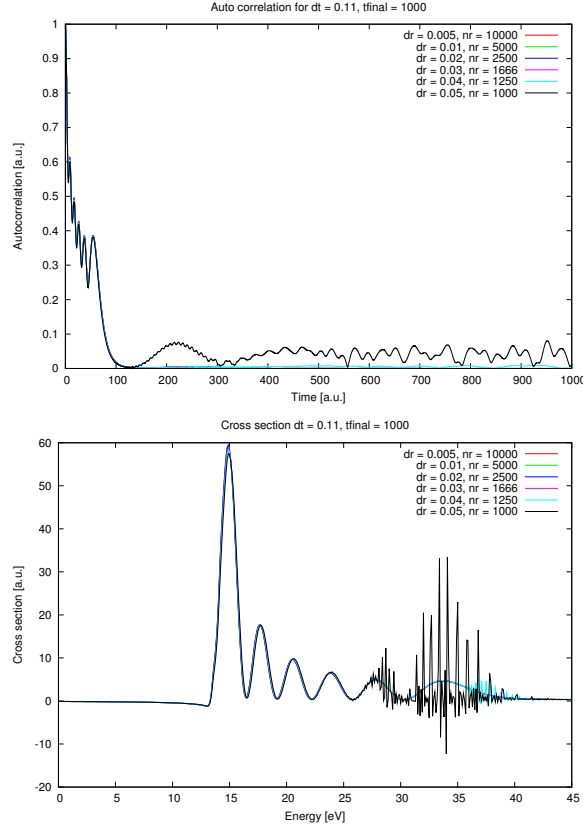


Figure 18: The autocorrelation and the cross section calculated for different dr . We can see that the result becomes unstable for dr larger than 0.3.

On the other hand, when investigating the step size on the R-grid, we notice that the convergence for large dr , is quite poor. From Fig. 18, it can be seen that the wave packet propagation exhibits a very unstable behavior for step sizes slightly larger than 0.3 (atomic length units).

The reason for this instability can be explained theoretically using a rough model. As the wave packet is constituted of quantum mechanical waves, the *de Broglie wavelength*, λ_{db} , can be used to connect the momentum of the wave packet to the energy domain. The de Broglie wavelength is connected to the momentum, p , of a particle by the *de Broglie equation*⁶

$$p = \frac{2\pi}{\lambda_{\text{db}}}, \quad (\text{B.1})$$

The kinetic energy, E , connected to this momentum is given as

$$E = \frac{p^2}{2\mu}, \quad (\text{B.2})$$

⁶Observe that atomic units are used, hence $\hbar = m_e = e = 1$.

where μ is the reduced mass. Assuming that to resolve a wave at least five grid-points are needed within a wavelength, *i.e.* $\lambda_{\text{db}} \sim 5dr$, E_{max} , for a certain dr can be estimated using Eqs. (B.1) and (B.2). In table (B.1) E_{max} for some values of dr are displayed. μ is taken as the reduced mass of the system, for HeH^+ $\mu = 0.8 \times 1822.9 m_e$.

Table B.1: E_{max} for different dr . The step size and the momentum are given in atomic units.

dr	p	E_{max} (eV)
0.01	125.66	147.33
0.02	62.83	36.83
0.03	41.89	16.37
0.04	31.42	9.21
0.05	25.13	5.89

The energy span for which our model will be applied is 15 – 38.9 eV (total energy). However, no numerical instabilities are visible for $dr = 0.02$ and $dr = 0.03$ although, we can see in table (B.1) we should use a $dr < 0.02$ in order to get proper resolution of the wave packet. The reason for this could be that the calculation is not that sensitive as we have not yet introduced the T-matrix elements. Therefore, we will choose to use $dr = 0.01$ in our calculations in order to assure full resolution.

C Appendix III - Conventions and notations

Table C.1: Energy, length and time conversions

Quantity	Value au	Conversion
Energy	1 E_h	27.21139 eV
Length	1 a_0	0.529177 Å
Time	1 $a_0/(\alpha c)$	2.41889×10^{-17} s

Table C.2: Fundamental Constants given in SI and atomic units (au).

Quantity	Symbol	Value and unit SI	Value au	Expression
Speed of light	c	2.99792×10^8 m/s	137.036	$= \alpha^{-1}$
Planck's constant	\hbar	1.05457×10^{-34} Js	1	$= h/2\pi$
Elementary charge	e	1.60218×10^{-19} C	1	
Mass of electron	m_e	9.10938×10^{-31} kg	1	
Permittivity of space	ϵ_0	8.85418×10^{-12} C ² /Jm	1/4π	
Boltzmann constant	k_B	1.38065×10^{-23} J/K		
Fine structure constant	α	1/137.036	1/137.036	$= e^2/(4\pi\epsilon_0\hbar c)$
Bohr radius	a_0	5.29177×10^{-11} m	1	$= \hbar/(\alpha m_e c)$

Table C.3: Functions

Symbol	Significance
$\Psi(\mathbf{R}, t)$	Wavefunction of TDSE
$\psi(\mathbf{R})$	Wavefunction of TISE
$U(R)$	Potential function
$\sigma(\omega)$	Cross section
$\Sigma(\omega)$	Cross section (alternative) [15]
$\delta(t)$	Dirac delta function
$A(t)$	Autocorrelation function

Table C.4: Operators

Symbol	Significance	Expression
∇^2	Laplace operator	$\nabla^2 = \frac{\partial^2}{\partial X^2} + \frac{\partial^2}{\partial Y^2} + \frac{\partial^2}{\partial Z^2}$
\mathcal{F}	Fourier operator	$\mathcal{F}\{f(t)\} = \int_{-\infty}^{\infty} f(t)e^{-i\omega t} dt$
\mathcal{F}^{-1}	Inverse Fourier operator	$\mathcal{F}^{-1}\{\tilde{f}(t)\} = \int_{-\infty}^{\infty} \tilde{f}(t)e^{-i\omega t} dt$

Table C.5: Notation

Symbol	Significance	Expression
i	Imaginary unit	$i^2 = -1$
μ	Reduced mass	$\mu = m_1 m_2 / (m_1 + m_2)$
λ_{db}	De Broglie wavelength	$\lambda_{\text{db}} = h/p$

References

- [1] M. Larsson and A. E. Orel, *Dissociative Recombination of Molecular Ions* (Cambridge University Press, New York, 2008), first edition, pp. 288-293.
- [2] A. E. Orel, T. N. Rescigno and B. H. Lengsfeld III, *Phys. Rev. A* **44**, 4328 (1991).
- [3] F. B. Yousif and J. B. A. Mitchell, *Phys. Rev. A* **40**, 4318 (1989).
- [4] C. Strömholm, J. Semaniak, S. Rosén, H. Danared, S. Datz, W. van der Zande and M. Larsson, *Phys. Rev. A* **54**, 3086 (1996).
- [5] A. E. Orel and K. C. Kulander, *Phys. Rev. A* **54**, 4992 (1996).
- [6] J. Royal and A. E. Orel, *Phys. Rev. A* **75**, 052706 (2007).
- [7] D. M. Chase, *Phys. Rev.* **104**, 838 (1971).
- [8] D. E. Golden, N. F. Lane, A. Temkin and E. Gerjuoy, *Rev. Mod. Phys.* **43**, 642 (1971).
- [9] M. Shugard and A. U. Hazi, *Phys. Rev. A* **12**, 1895 (1975).
- [10] T. N. Rescigno, C. W. McCurdy, A. E. Orel and B. H. Lengsfeld III, *Computational Methods for Electron-Molecule Collisions*, ed. by W. M. Huo and F. A. Gianturco (Plenum Press, New York 1995).
- [11] M. Born and R. Oppenheimer, *Ann. Phys.* **84** 457 (1927).
- [12] J. von Neumann and E. P. Wigner, *Z. Phys.* **30** 467 (1929).
- [13] C. W. McCurdy, T. N. Rescigno and B. I. Schneider, *Phys. Rev. A* **36**, 2061 (1987).
- [14] B. I. Schneider and T. N. Rescigno, *Phys. Rev. A*, **37**, 3749 (1988).
- [15] E. J. Heller, *J. Chem. Phys.* **68**, 2066 (1978).
- [16] E. J. Heller, *J. Chem. Phys.* **68**, 3891 (1978).
- [17] D. J. Tannor, *Introduction to quantum mechanics, a time-dependent perspective* (University Science Books, Sausalito, CA, 2007), first edition.
- [18] A. Goldberg, H. M. Shey and J. L. Schwartz, *Am. J. Phys.* **35**, 177(1967).

- [19] D. E Woon and T. H. Dunning, Jr., *J. Chem. Phys.* **100**, 2975 (1994).
- [20] T. H. Dunning, Jr., *J. Chem. Phys.* **90**, 1007 (1989).
- [21] G. B. Arfken and H. J. Weber, *Mathematical methods for physicists* (Elsevier Academic Press, Burlington, MA, 2005), sixth edition.
- [22] A. Prosperetti, *Advanced Mathematics for Applications* (Cambridge University Press, New York, 2011), first edition.